The Mw = 6.3, November 21, 2004, Les Saintes earthquake (Guadeloupe): Tectonic setting, slip model and static stress changes,

Nathalie Feuillet, François Beauducel, E. Jacques, Paul Tapponnier, B. Delouis, S. Bazin, Martin Vallée, G.C.P. King

The Mw = 6.3, November 21, 2004, Les Saintes earthquake (Guadeloupe): Tectonic setting, slip model and static stress changes

N. Feuillet,[1] F. Beauducel,[1] E. Jacques,[1] P. Tapponnier,[2] B. Delouis,[3] S. Bazin,[1,4] M. Vallée,[3] and G. C. P. King[1]

Received 17 February 2011; revised 17 June 2011; accepted 30 June 2011; published 4 October 2011.

[1] On November 21, 2004, a magnitude 6.3 earthquake occurred offshore, 10 km south of Les Saintes archipelago in Guadeloupe (French West Indies). There were more than 30000 aftershocks recorded in the following two years, most of them at shallow depth near the islands of the archipelago. The main shock and its main aftershock of February 14, 2005 (M_w = 5.8) ruptured a NE-dipping normal fault (Roseau fault), mapped and identified as active from high-resolution bathymetric data a few years before. This fault belongs to an arc-parallel en echelon fault system that follows the inner edge of the northern part of the Lesser Antilles arc, accommodating the sinistral component of oblique convergence between the North American and Caribbean plates. The distribution of aftershocks and damage (destruction and landslides) are consistent with the main fault plane location and attitude. The slip model of the main shock, obtained by inverting jointly global broadband and local strong motion records, is characterized by two main slip zones located 5 to 10 km to the SE and NW of the hypocenter. The main shock is shown to have increased the Coulomb stress at the tips of the ruptured plane by more than 4 bars where most of the aftershocks occurred, implying that failures on fault system were mainly promoted by static stress changes. The earthquake also had an effect on volcanic activity since the Boiling Lake in Dominica drained twice, probably as a result of the extensional strain induced by the earthquake and its main aftershock.

Citation: Feuillet, N., F. Beauducel, E. Jacques, P. Tapponnier, B. Delouis, S. Bazin, M. Vallée, and G. C. P. King (2011), The Mw = 6.3, November 21, 2004, Les Saintes earthquake (Guadeloupe): Tectonic setting, slip model and static stress changes, *J. Geophys. Res.*, *116*, B10301, doi:10.1029/2011JB008310.

1. Introduction

[2] On November 21, 2004, at 11:41 UT, the archipelago of Les Saintes in Guadeloupe (French West Indies) was struck by a M_w = 6.3 earthquake [*Beauducel et al.*, 2005]. Except for the November 2007 M_w = 7.4 intermediate earthquake in Martinique [*Bazin et al.*, 2008], this event was the strongest recorded in the French territory islands for more than a century.

[3] The earthquake occurred offshore between Les Saintes and Dominica islands (Figure 1b). Several magnitude $M_w \approx$ 5.0 aftershocks followed the main shock. Two of them reached magnitudes of 5.3 in the following hours, and were followed by a M_w = 4.9 shock on November 27, and a M_w = 5.0 on December 2. On February 14, 2005 an earthquake of M_w = 5.8 occurred north of the November 21 shock. The last large aftershock (M_w = 4.8) was recorded on June 6, 2005. The aftershock sequence continued into 2008, with more than 30000 aftershocks having been recorded by the regional seismic networks of Guadeloupe and Martinique [*Institut de Physique du Globe de Paris* (*IPGP*), 2008]. Many were felt by Les Saintes inhabitants, not only those with magnitudes greater than 4, but frequently shallower ones with magnitudes 2 or 3. The main shock reached an intensity of VIII in Les Saintes, where it caused much damage, with one fatality in Guadeloupe [*Cara et al.*, 2005], and triggered a small tsunami [*Le Friant et al.*, 2008]. Today, several clusters of small earthquakes are still recorded beneath the Saintes islands.

[4] Earthquakes of this magnitude are infrequent in the Lesser Antilles arc, where two types of seismic events are routinely recorded: thrust events related to subduction on the interface between the Caribbean and American plates and shallow normal or strike-slip intraplate events within the arc [*Feuillet et al.*, 2004]. The last intraplate event of comparable magnitude was the Redonda earthquake, on March 16, 1985, between Montserrat and Nevis [*Feuillet et al.*, 2010].

[1]Institut de Physique du Globe de Paris, Sorbonne Paris Cité, UMR 7154, CNRS, Université Paris Diderot, Paris, France.
[2]Earth Observatory of Singapore, Nanyang Technological University, Singapore.
[3]GéoAzur, Université de Nice Sophia-Antipolis, IRD, CNRS, OCA, Valbonne, France.
[4]Now at Norwegian Geotechnical Institute, Oslo, Norway.

0148-0227/11/2011JB008310

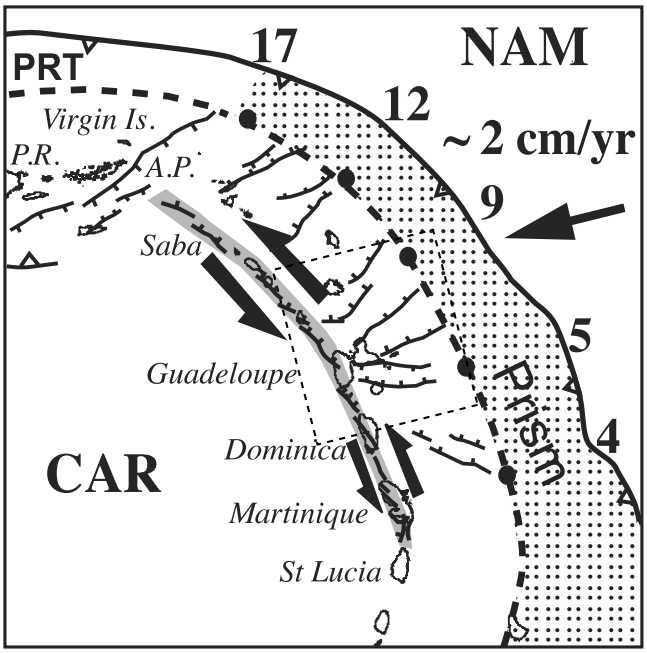

Figure 1a. Simplified map showing the link between en echelon inner Lesser Antilles arc fault system and subduction. Black dots with numbers: values of trench parallel component of shear (increasing from 4 to 17 mm/yr between Martinique and Anegada Passage (A.P.)) calculated by using the new Caribbean North American Euler vector of *Lopez et al.* [2006]. Gray line with arrows: inner en echelon fault system with slip probably increasing northward. Hatched area: accretionary wedge, G: Guadeloupe, M: Martinique, V.I.: Virgin Islands, P.R. Puerto Rico, PRT: Puerto Rico trench. Black line with triangles: frontal thrust. Dashed *black* line: main negative gravity anomaly (trench) from *Bowin* [1976]. CAR: Caribbean Plate, NAM: North American plate.

This paper presents a multidisciplinary seismotectonic study of the Saintes earthquakes that occurred along a fault identified as active and mapped as part of an offshore normal fault system crossing the Les Saintes channel during the marine geophysical survey AGUADOMAR 1998–1999 [*Feuillet*, 2000; *Deplus et al.*, 2001].

[5] We first present a detailed map of active faults between Les Saintes and Dominica as well as observations and measurements performed in the field a few weeks after the earthquake and have deduced which fault may have ruptured during the earthquake. We also relocate the main shock as well as six main aftershocks in order to better assess the source of the earthquake. The coseismic slip distribution is obtained from the joint inversion of teleseismic and strong motion records and further validated by the Empirical Green's Function (EGF) approach. Static stress changes are then modeled to account for occurrence and distribution of aftershocks.

[6] We also document the hydrological effects of the earthquake on the neighboring Boiling Lake in Dominica. A complete study on volcanoes and earthquakes interactions is beyond the scope of this paper but is the main purpose of a separate paper [*Feuillet et al.*, 2011] in which we document, through statistical analysis and static stress models, the link between the larger historical earthquakes and the volcanic activity in the arc.

2. Active Faulting and Seismicity in the Northern Lesser Antilles Arc

[7] Part of the Lesser Antilles arc between St Lucia and Antigua was surveyed by the French R/V l'Atalante in December 1998–January 1999 (AGUADOMAR cruise). The data acquired included multibeam Simrad EM12D/1000 swath bathymetry and backscatter, 3.5 khz echosounder, 6-channel seismic reflection, magnetic and gravimetric data along 242 profiles extending up to 70 km from the islands [*Deplus et al.*, 2001]. The use of Starfix differential GPS allowed the ship to be located to within a few meters. Digital terrain models (DTM) with resolutions of 50, 100 and 200 m were created on board and later at Institut de Physique du Globe de Paris using the IFREMER CARAIBE software. The DTM vertical accuracy decreases with depth and is about 10 m at 5000 m bsl. For safety reasons, no data could be acquired by the large vessel in very shallow water (<50 m). Between Les Saintes and Dominica, however, we were able to complement the AGUADOMAR data with shallow bathymetry acquired by the hydrographic service of the French national marine (SHOM). On land, we used the French National Geographic Institute (IGN) and SRTM3 topographic data in Guadeloupe and Dominica, respectively. Seismic profiles perpendicular to the scarps help constrain the geometry of the fault system at depth in cross-section.

[8] Figure 1b shows the main active fault systems mapped at the scale of the arc between Antigua and Dominica [*Feuillet et al.*, 2004] and the main shallow earthquakes (depth < 30 km, $M > 3.5$) recorded by the IPGP observatories since 1981. The northern part of the Lesser Antilles arc is the site of trench parallel extension, which is accommodated by trench-perpendicular, normal or oblique faults [*Feuillet*, 2000; *Feuillet et al.*, 2002, 2004]. These faults cut the outer, eastern edge of the overriding Caribbean plate. Some show cumulative scarps several kilometers long and several tens of meters high that form sharp, steep steps in the topography and bathymetry. Accurate mapping of such escarpments both on land and offshore provides an overview of the geometry and kinematics of faulting at a range of scales (Figures 1b and 2). Overall, these intraplate faults, which are responsible for much of the shallow seismicity recorded in the arc, appear to form two distinct sets (Figure 1b). Faults belonging to the first set bound arc-perpendicular graben or half graben that disrupt the fore-arc reef platforms of Grande-Terre, Marie-Galante and La Désirade. Such graben can be up to 100 km-long and 50 km-wide. The Marie-Galante graben, in particular, cuts the Guadeloupe archipelago, separating Grande-Terre from Marie-Galante. Faults along this graben have produced one damaging $M \approx 5.5$ earthquake on May 16th, 1851, southeast of Basse-Terre. According to *Bernard and Lambert* [1988], they might have also been the source of the April 29, 1897 earthquake, with an epicenter near Pointe-à-Pitre and a magnitude of about 5.5.

[9] The faults of the second set are 5 to 20 km long, strike N145 ± 15°E and form right-stepping en echelon arrays. Such oblique normal fault arrays appear to accommodate

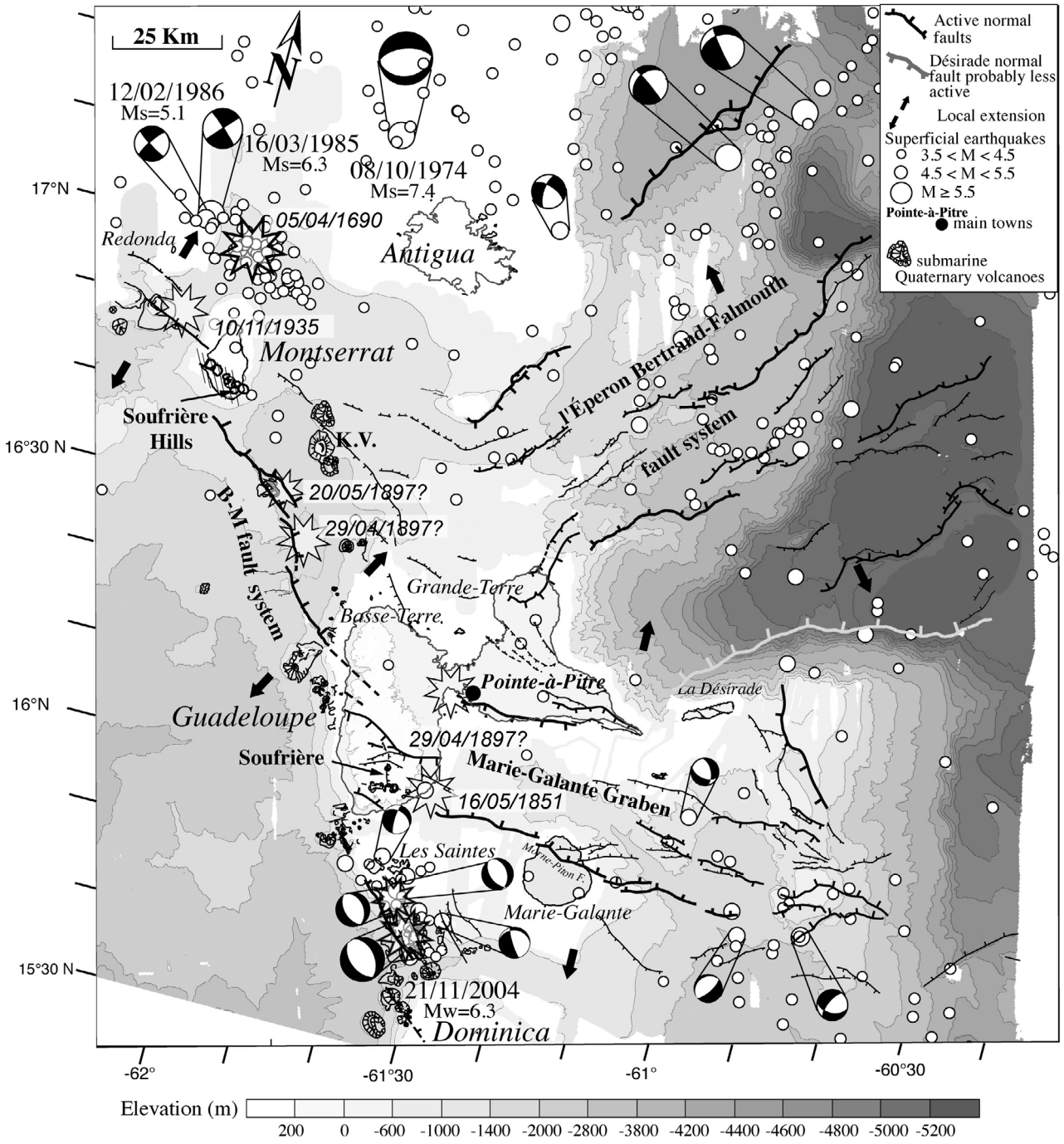

Figure 1b. Seismotectonic map of the northern Lesser Antilles arc between Dominica and Antigua. Topography from French "Institut Géographique National" DEM. High-resolution multibeam bathymetry redrawn from AGUADOMAR cruise DEM. Contours at 200 m interval. Active faults in black with ticks from *Feuillet* [2000], *Feuillet et al.* [2001, 2002, 2004, 2010]. Double black arrows: local direction of extension deduced from fault geometry and focal mechanisms. White dots: 1981–2006, shallow (<30 km) seismicity from bulletins of volcanological observatories of Guadeloupe and Martinique (Institut de Physique du Globe de Paris). Focal mechanisms of main intraplate earthquakes, with dates from *Stein et al.* [1982], *McCann* [1985], *Dziewonski et al.* [2000]. Stars: location of $I \geq$ VII ($M \geq 6$) earthquakes with dates from *Robson* [1964], *Feuillard* [1985], *Bernard and Lambert* [1988], and this study. The 1897 earthquake epicenter in NW Basse-Terre from *Feuillard* [1985]. Quaternary volcanoes in grey. Hatched area in southern part of Montserrat: most recent volcanic complex.

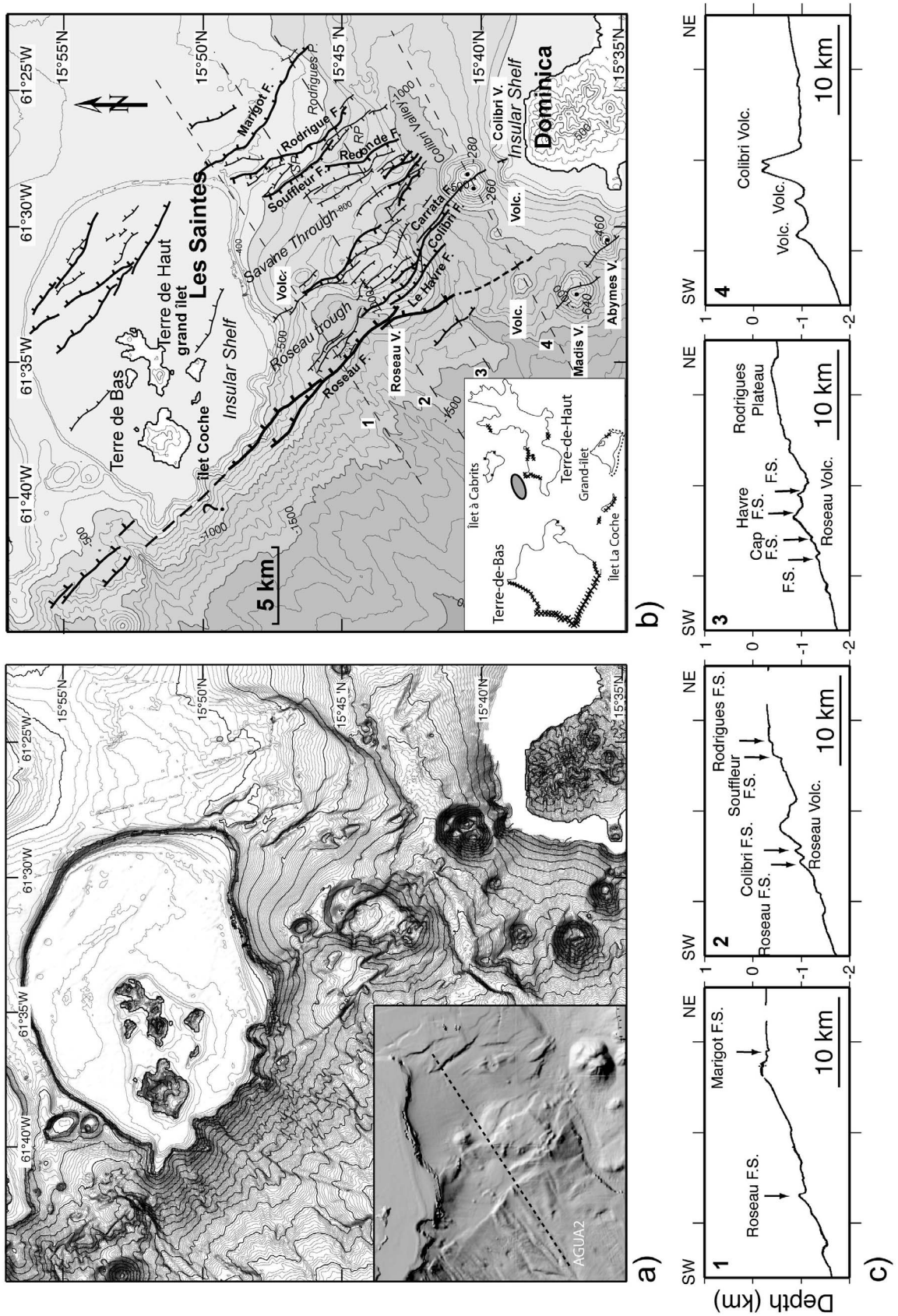
a)
b)
c)
Les Saintes
Terre de Haut
Terre de Bas
grand îlet
îlet Coche
Insular Shelf
Savane Through
Roseau trough
Roseau F.
Roseau V.
Volc.
Marigot F.
Rodrigue F.
Rodrigues P.
Souffleur F.
Reconde F.
Colibri Valley
Carrata F.
Colibri F.
Le Havre F.
Colibri V.
Dominica
Abymes V.
Madis V.
5 km
Îlet à Cabrits
Terre-de-Bas
Terre-de-Haut
Grand-îlet
Îlet La Coche
AGUA2
Depth (km)
SW
NE
Roseau F.S.
Marigot F.S.
Colibri F.S.
Souffleur F.S.
Rodrigues F.S.
Roseau Volc.
Cap F.S.
Havre F.S.
Rodrigues Plateau
Colibri Volc.
10 km

Figure 2

left-lateral transtension along the inner, volcanic islands between Les Saintes and Redonda (Figure 1b). This en echelon system cuts the active volcanoes of Soufrière de Guadeloupe and Soufriere Hills of Montserrat, as well as submarine volcanoes offshore [*Feuillet et al.*, 2001]. The main fault segments dip to the northeast, have recent, steep scarps up to 200 m high, and offset sedimentary layers by more than 400m between Basse-Terre and Montserrat [*Feuillet*, 2000; *Feuillet et al.*, 2010]. New high-resolution marine data obtained in March 2009 (GWADASEIS cruise, R/V le Suroit IFREMER) show that the inner-arc fault system continues northwestward crosscutting Saba, the northernmost volcanic island. It could extend toward the Virgin Islands, all the way to the Anegada passage [*Feuillet*, 2000] (Figure 1a). The GWADASEIS data also show that this fault system probably ends in the St Lucia channel, between Martinique and St Lucia (N. Feuillet et al., manuscript in preparation, 2011).

[10] In the last two decades, the inner arc en echelon fault system has been the source of two magnitude 6.3 earthquakes (March 16, 1985, Redonda earthquake, and November 21, 2004, Les Saintes earthquake).

[11] At plate scale, *Feuillet et al.* [2002] interpreted the arc-perpendicular fore-arc graben and inner-arc en echelon system to be connected, forming a sinistral horsetail east of the tip of the left-lateral Puerto Rico fault zone that takes up the trench-parallel component of convergence between the North-American and Caribbean plates west of the Anegada passage (Figure 1a). Based on a morphotectonic analysis of uplifted marine terraces dated with U/Th in Marie-Galante, a slip-rate on order of 1 mm/yr was determined for the Morne-Piton fault, which bounds the Marie-Galante graben to the south [*Villemant and Feuillet*, 2003; *Feuillet et al.*, 2004]. Such a slip-rate would be consistent with a magnitude 6.5 earthquake every 1500–3000 yrs. Although there is no direct slip-rate measurement yet on faults along the inner-arc fault system, large scale partitioning of plate boundary motion suggests a total of a few mm/yr across the entire system. Such rates are large enough that seismic hazard from shallow sources within the arc should be considered significant compared to that related to megathrust earthquakes along the plate interface. In Guadeloupe, upper plate active faults can be 30–50 km long. Since earthquake magnitudes scale with fault length [*Wells and Coppersmith*, 1994], the occurrence of upper-plate, $M > 6$ earthquakes, comes as no surprise. The possible occurrence of even larger events, such as the tsunamigenic, 1867 Virgin Islands earthquakes [*Reid and Taber*, 1920] or the Antigua event of the October 8, 1974 (M_s = 7.4 [*McCann et al.*, 1982]), in the northern part of the arc, may be due to such faulting.

3. Les Saintes Channel Fault System

[12] Figure 2a shows the digital terrain model (DTM) with a resolution of 50 m between Basse-Terre and Dominica, in the area struck by the November 21, 2004 earthquake. During the 1998–1999 AGUADOMAR cruise, only two seismic profiles were acquired in this area. Profile number 2 perpendicular to the fault system is shown in Figure 3.

[13] The seafloor is disrupted by numerous arc-parallel normal faults, with steep scarps several tens of meters high that cut across or interrupt all other bathymetric features, as is typical of sustained, active fault motion (Figures 2 and 3). The faults form a NW-SE striking graben, that represents the southern continuation of the right-stepping, N140°E-striking, Bouillante-Montserrat faults array. They offset vertically the Rodrigues, Souffleur, and Redonde submarine plateaus and Savane and Roseau troughs, at depths ranging between 400 and 1100 m, as well as the Roseau, Colibri, Madis, and Abymes volcanic cones that belong to the recent arc. The largest of these submarine volcanoes is the Roseau volcano. Extensional downthrow clearly postdates fairly recent volcanic construction, as attested by the well-preserved shapes and seismic profile AGUA02 (Figure 3). Although the exact ages of the volcanoes are not known, direct dating of lavas in adjacent northern Dominica and Les Saintes suggests upper Pliocene-Quaternary activity [*Bellon*, 1988; *Jacques and Maury*, 1988].

[14] The largest fault (Roseau fault) bounds the west side of the Les Saintes channel graben. It is 15 km-long, with a cumulative scarp height of up to 120 m. It strikes N135 ± 15°E on average, dips northeastward and is associated with shorter antithetic faults (2–10 km-long, Rodrigues, Souffleur, Redonde) on the opposite side of the graben (Figure 3). Another fault segment probably takes over in right-stepping fashion along the western edge of Les Saintes insular shelf, connecting with the active faults identified southwest of Basse-Terre but the shallow bathymetry's resolution is insufficient to demonstrate this. To the south, the Roseau fault continues as a left-stepping array of normal faults (Le Havre, Colibri and Carrata). The N150 ± 20°E striking west-dipping faults bounding the graben to the east have scarps up to 140 m-high. They form a right-stepping array along the N0 ± 10°E direction. East of Terre-de-Haut, the Les Saintes insular shelf is cut by N130 ± 10°E-striking, northeastward-

Figure 2. Detailed map of active faults between Basse-Terre and Dominica. Topography is from IGN and SRTM, for Guadeloupe and Dominica, respectively. Bathymetry as in Figure 1b. Shallow bathymetry (<50 m) is from SHOM (reproduction authorization number 275/2011, SHOM hydrographic service of the French national marine, Warning: The SHOM, and any other official hydrographic service cannot be held for responsible of the results published in this study). (a) Map with contours at 10 m vertical intervals (thicker traces at 100 m intervals) and shaded bathymetry in inset (illumination from NE). (b) Tectonic interpretation. Contours at 100 m vertical intervals with thicker traces at 500 m intervals. Active normal faults are in black with ticks on the downthrown side, with thicker traces for larger faults. Dashed black lines, position of topographic cross-sections with numbers shown in Figure 2c. RP: Rodrigue plateau, SP: Souffleur plateau, V or Volc: Volcano, F: Fault, Figure 2b inset: Location of coastal landslides triggered by November 21 2004, earthquake, with larger crosses for larger landslides. All coasts were explored except the southern coast of Grand-Îlet (dashed line). Gray ellipse: location of white patch in seawater described by inhabitants of Les Saintes (see text and photograph on Figure 5). (c) Bathymetric cross-sections along profiles shown in Figure 2b. F.S.: fault scarp, Volc: volcano.

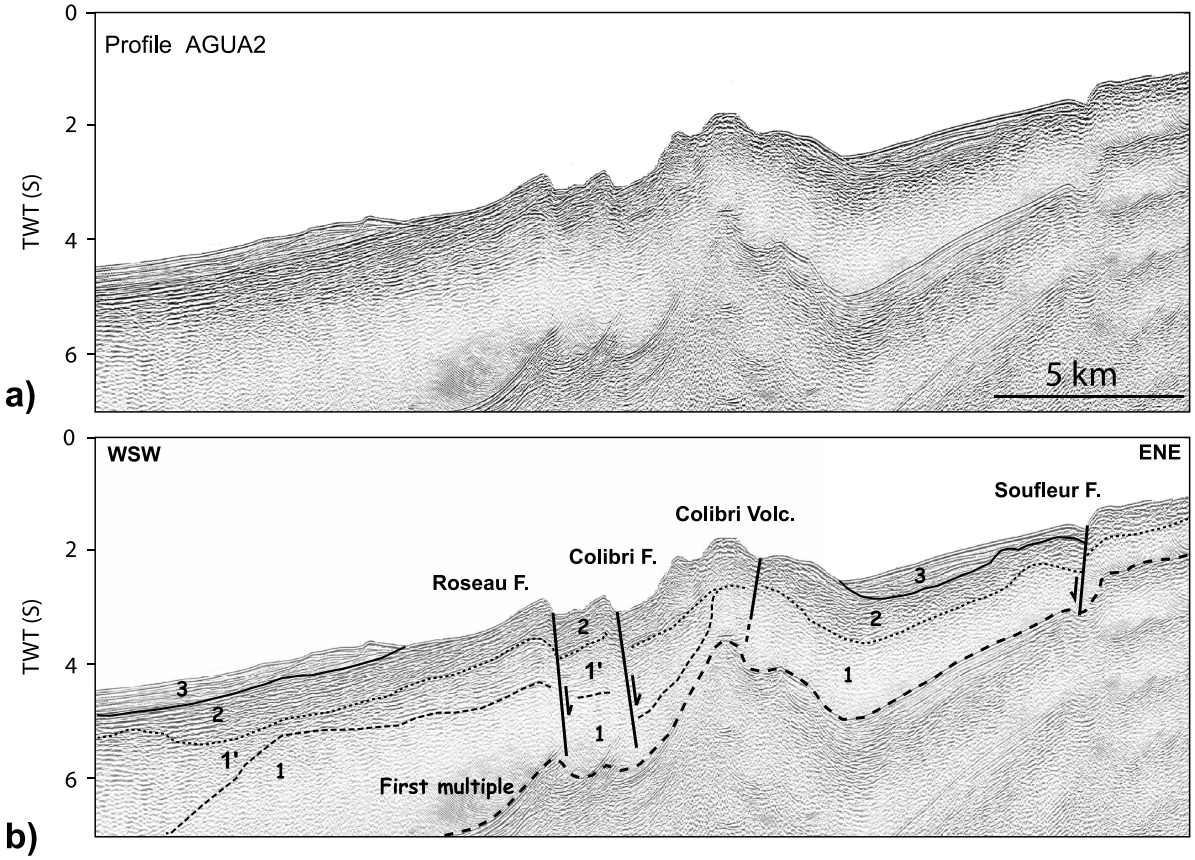

Figure 3. (a) A 6 channel seismic profile (AGUA2) acquired during the AGUADOMAR marine cruise, crossing the Les Saintes channel, active faults and volcanoes (location on Figure 2a inset). (b) Interpretation: Three to four main sedimentary units can be identified (1, 1′, 2 and 3). All cut by the Les Saintes graben faults (Roseau, Colibri, Souffleur) up to seafloor, attesting for recent activity.

dipping active faults with scarps up to 12 m-high, probably linked with other similar faults (e.g., Marigot fault) to the south. NE directed extension between Les Saintes and La Dominica is consistent both with the faulting geometry observed and with the regional kinematics (Figures 1a, 1b, and 2).

4. Localization of the November 21, 2004 Main Shock and Its Aftershocks

[15] The November 21, 2004 magnitude 6.3 earthquake clearly ruptured one of the Les Saintes channel graben faults. The empirical relationship of *Wells and Coppersmith* [1994], which relates surface rupture length to Moment magnitude, is consistent with a fault plane length of about 15–20 km. As commonly observed with extensional faulting in volcanic regions [*Jacques et al.*, 1999, 2011], the main shock was followed by several aftershocks of magnitude close to 5. The largest one (M_w = 5.8) occurred on February 14, 2005, north of the 21 November shock.

[16] A detailed seismological analysis of the Les Saintes earthquake series being beyond the scope of this paper, we relocated only the main shock and the six largest aftershocks ($4.9 < M_w < 5.8$) for which a Harvard focal mechanism [*Dziewonski et al.*, 2000] is available. We used the HYPO71 code [*Lee and Lahr*, 1975] with *Dorel* [1978] 1-D velocity model, derived from seismic refraction profiles, to invert the P and S arrival times picked and validated by the CDSA (French Antilles Seismological Data Base) [*Bengoubou-Valerius et al.*, 2008]. We used the V_p/V_s ratio of 1.75 determined by *Duclos et al.* [2007]. Station distance weighting is equal to 1 when the station is less than 70 km from the epicenter and decreases linearly to 0 for stations more than 120 km from the epicenter. Some stations (accelerometers and short period seismometers, mostly located in eastern Guadeloupe and in Marie-Galante) were not taken into account for location because P and S travel time residuals calculated at these stations were too large (>1 s). Similarly large residuals were also obtained at these stations for smaller aftershocks in the Les Saintes channel (M. P. Bouin, personal communication, 2007).This may be due to fairly large velocity anomalies across the fault system. Our results are shown in Table 1 and Figure 4. The computed hypocentral locations have mean horizontal and vertical errors of 1.1 km and 1.3 km, respectively, and a root mean square (RMS) residual of 0.22 s. All events lie within the seismic network with gaps of less than 155° in station coverage. The main shock occurred at 10 km depth within Les Saintes fault system. Its hypocentral location is compatible with a mean dip of 50° for the Roseau fault, in agreement with the focal mechanism. It seems to have occurred close to the connection at depth between the Roseau and Redonde faults (Figure 4c,

Table 1. Main Shock and Aftershocks Relocations and Focal Mechanisms

Name	Date	Hours	Mw[a]	Lat (°N)	Lon (°W)	depth (km)	RMS	Gap (deg)	ERH	ERZ	Q	Strike[a] (deg)	Dip[a] (deg)	Rake[a] (deg)
MS	2004-11-21	11:41:08	6.3	15°45.88	61°30.12	10.0	0.22	144	0.9	0.8	C1	325	44	−77
AFT1	2004-11-21	13:37:00	5.3	15°46.30	61°30.07	9.5	0.23	143	0.7	0.8	C1	264	22	−53
AFT2	2004-11-21	18:53:03	5.3	15°50.05	61°33.67	8.8	0.22	151	1.7	2.1	C1	331	41	−74
AFT3	2004-11-27	23:44:24	4.9	15°42.39	61°30.21	9.2	0.24	147	0.8	0.8	C1	289	41	−160
AFT4	2004-12-02	14:47:54	5.0	15°45.16	61°29.74	10.6	0.27	131	1.8	1.7	B1	296	39	−123
AFT5	2005-02-14	18:05:59	5.8	15°49.44	61°33.30	9.0	0.14	155	1.2	2.7	C1	324	39	−84
AFT6	2005-06-06	01:20:06	4.8	15°49.10	61°32.08	14.7	0.24	120	0.7	0.6	B1	286	53	−129

[a]Source: http://www.globalcmt.org/CMTsearch.html.

cross-section C). The six main aftershocks are located in two distinct zones within the graben at depths ranging between 9 and 14 km. The first and fourth aftershocks occurred very close to the main shock. The second and last aftershocks occurred 10 km farther north, very close to the main aftershock of February 14, 2005 (AFT5 on Figure 4). The focal mechanisms of all aftershocks indicate NW-striking normal faulting, compatible with the surface fault geometry and the regional NE extension.

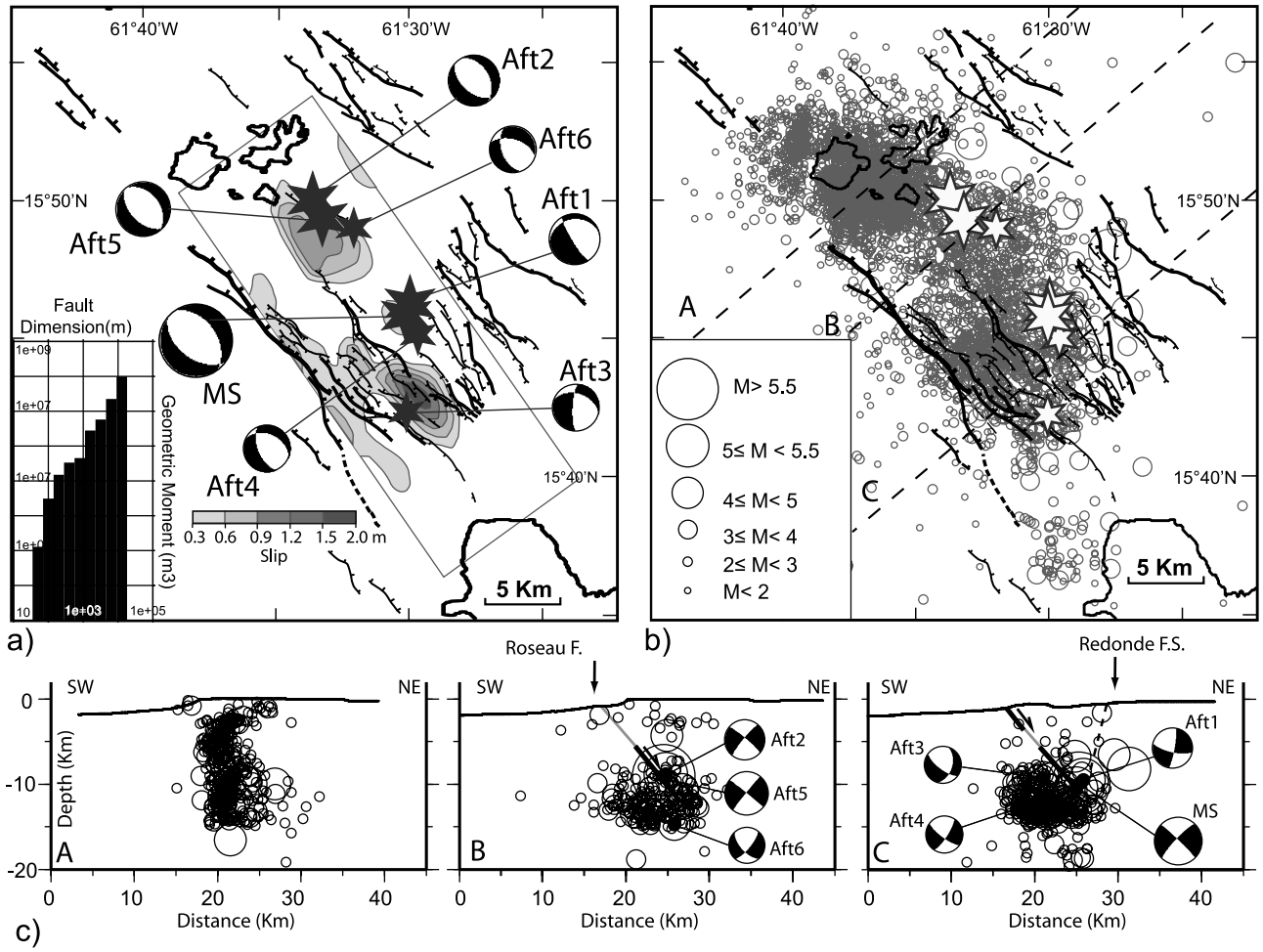

Figure 4. Location of seismic events recorded by Guadeloupe and Martinique observatories. Mean location errors are 2.7 km for epicenters position and 2.0 km for focal depth. Main shocks ($M_w > 5$) are shown by stars. Focal mechanisms are from Harvard catalogue [*Dziewonski et al.*, 2000], with names referring to Table 1. Faults as in Figure 2. Dashed lines, location of cross-sections A, B, C shown in Figure 4c. The surface projection of the slip model is shown with larger slip in darker gray. Inset in Figure 4a indicates geometric moment (potency) release as a function of fault dimension. (c) SW-NE seismic cross-sections (locations in Figure 4b) with focal mechanisms as in Figure 4a. Gray line: fault plane with portions in black showing the rupture zones. Dashed black line in cross-section C, Redonde fault plane deduced from seafloor scarp position and mechanism of first aftershock (Aft 1).

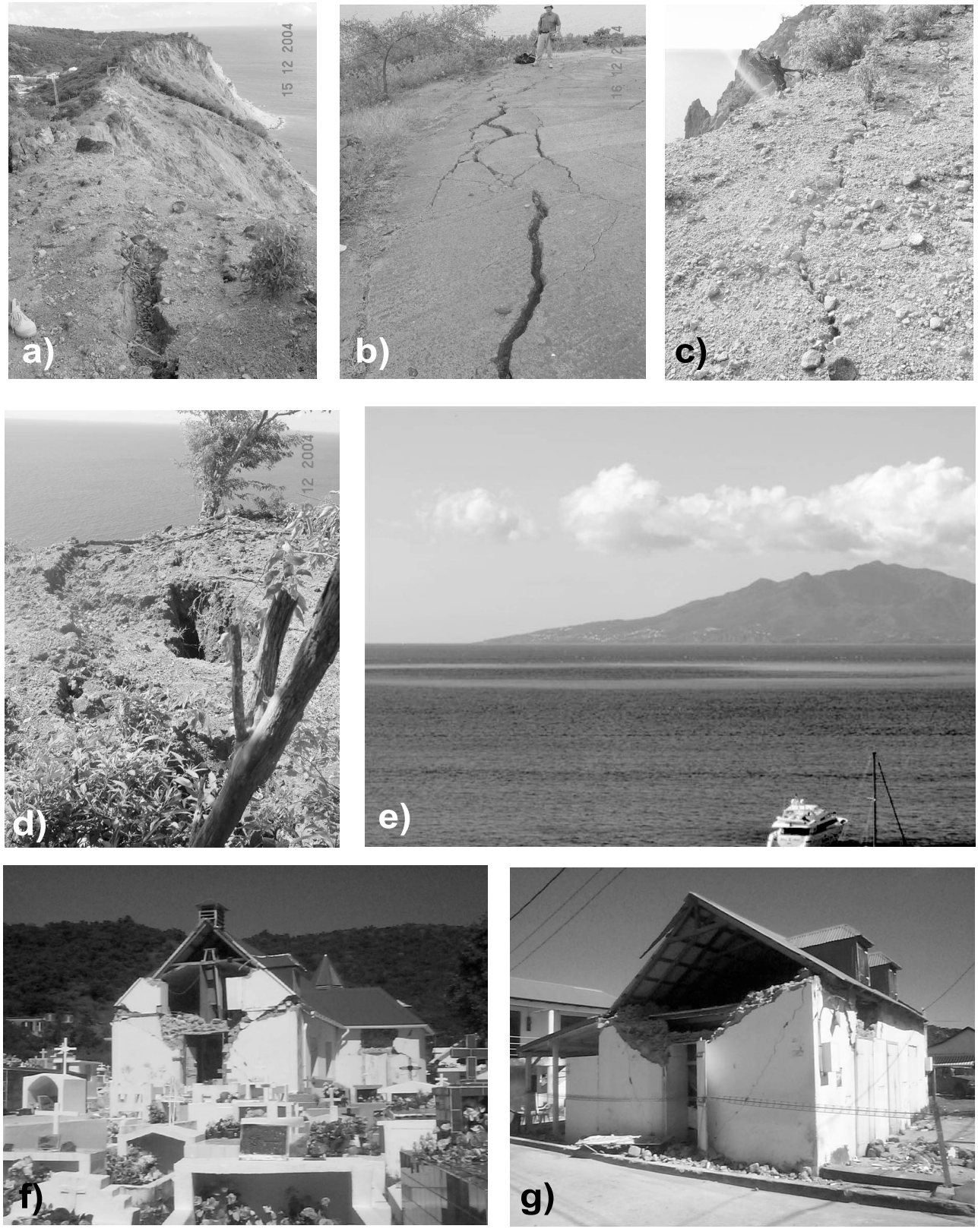

Figure 5. Field photographs of damage caused by November 21, 2004, $M \approx 6.3$ earthquake in Les Saintes archipelago. (a) Landslides and fissuring along southern coast of Terre-de-Bas. (b–d) Open fissures parallel to southern cliff of Terre-de-Bas. (e) White patch on the sea surface offshore Terre de Haut observed by residents after February 14, 2005 aftershock (Photograph: P. Bellenus, Terre de Haut). (f and g) Damaged buildings in Terre-de-Bas.

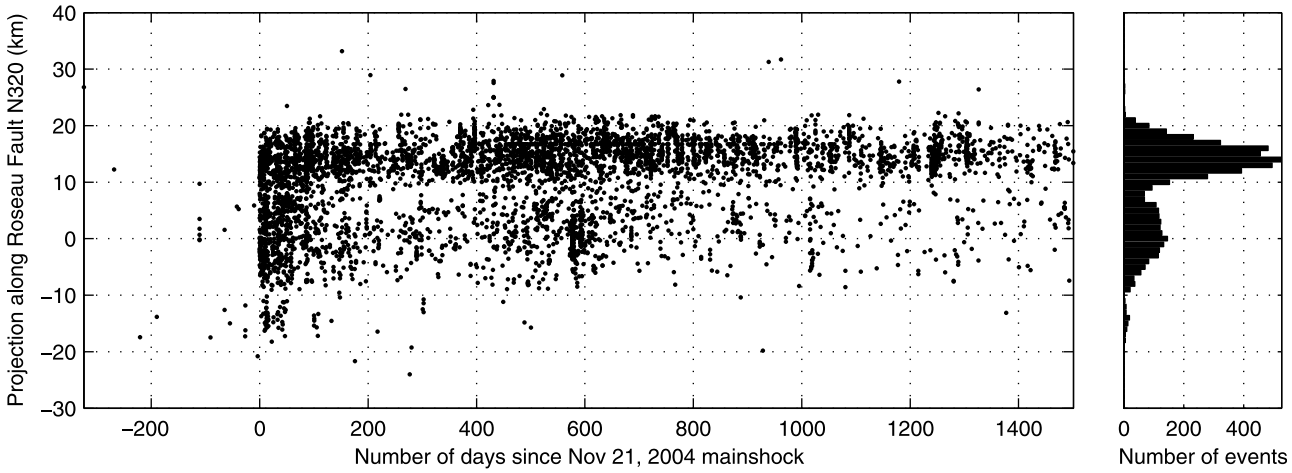

Figure 6. (left) Space-time evolution of aftershock distribution projected on direction parallel to the Roseau fault between Basse-Terre and Dominica. (right) Histogram of events, showing the few km-large gap between southern and northern aftershock zones.

[17] The main shock was preceded two minutes before by a foreshock of magnitude 3. A few days after the main shock, two of us (NF and EJ) went to assess damage and map co- and post-seismic cracks and landslides in the field. The inset in Figure 2b shows the distribution of the larger landslides in Terre-de-Haut, Terre-de-Bas and along the coast of smaller islands (Îlet Côche, Grand Îlet, Îlet Cabri). The main shock caused numerous landslides, the largest of which was located along the southern cliff of Terre-de-Bas (Figure 5a). We mapped several fissure sets parallel to this cliff (Figures 5a–5d). The largest fissures, with the widest opening ≥1 m were observed in the south and eastern parts of Terre-de-Bas. In this island, 50% of the buildings were seriously damaged (Figures 5f and 5g), and the maximum intensity was estimated to VIII [*Cara et al.*, 2005]. In Terre-de-Haut, the damage was less serious but nonetheless 66% of all constructions were affected.

[18] Together, all of these observations are in keeping with rupture of a fault located to the south and west of the westernmost island. Based on the expected rupture length (15–20 km), submarine bathymetry, fault kinematics, and location of landslides and cracks along the steep SE cliff of Terre-de-Bas, we conclude that the NE-dipping Roseau fault, which is the longest one in Les Saintes channel graben - hence that most capable of generating an $M_w = 6.3$ event - was the fault that slipped during the main shock in agreement with *Bazin et al.* [2010] and *Le Friant et al.* [2008].

[19] Since the main shock, the French Antilles observatories have recorded more than 30 000 events. Following Omori's law, their frequency decreased from 150 events per hour the first day to about 100 to 150 earthquakes per month in January 2007. In early 2007, the largest aftershocks had magnitudes ≈3, and less than 10 events per month were being felt by the population. Given the large amount of data recorded, the seismological analyses are still in progress. The seismic catalog is not complete for small (<3) magnitude events, particularly in the first months of the aftershock sequence. Figures 4b and 4c shows the spatial distribution of the ≈4000 aftershocks located by the French observatories. These locations are preliminary, with mean horizontal and vertical errors of 2.7 and 2.0 km, respectively. Figure 6 shows the evolution, in space and time, of aftershock occurrence along strike of the Roseau fault. No clear migration of seismicity is observed. During the first two months, aftershocks occurred along the entire length of the fault system. They subsequently tended to cluster near the northern and southern tips of the Roseau fault, beneath Les Saintes plateau and Roseau volcano, respectively. Two distinct, persistent clusters of seismic moment release, separated by a ≈5 km long seismic gap, are visible. Save for a one monthlong period about 600 days into the crisis, the southern cluster was less active than the northern one, whose southern and especially northern limits are sharply defined. After about twenty-five months, the southern cluster started to fade out while the northern one continued to be fairly active. In the last 2 years, the latter cluster was characterized by small sequences of tens of $M < 4$ earthquakes occurring mainly beneath Les Saintes archipelago, the last two in April and June 2008. There were very few events, if any, along the easternmost, east-dipping fault system (Marigot and NE Saintes insular shelf faults). To the south, a small number of events were recorded in the first three months just west of Dominica's northwestern tip. Events north of the Roseau fault, beneath the Les Saintes insular shelf, have depths between 0 and 15 km, and outline a steeply northeast-dipping planar zone (cross-section A on Figure 4). To the south, aftershocks cluster at greater depths between 10 and 15 km.

5. Source Model of the Main Shock ($M_w = 6.3$)

[20] We present here a new source model for the main shock determined from the joint inversion of teleseismic and strong motion records (data from the French national strong motion permanent network (RAP) available at http://www-rap.obs.ujf-grenoble.fr/, see details in Appendix A). A previous model was proposed by *Salichon et al.* [2009] from the inversion of the teleseismic data only. Here we add the available strong motion records at distances less than 50 km in a joint inversion to increase the resolution on the rupture slip model and determine the optimum focal mechanism.

[21] The fault geometry was varied in a series of joint inversions until it was established that (strike, dip, rake) = (325, 55, −85) or (154, 35, −97) provided the best waveform fit of the two data sets. The plane dipping to the NE (325, 55, −85) was assumed to be the fault plane in agreement with rupture along the Roseau fault [*Bazin et al.*, 2010; *Le Friant et al.*, 2008]. Kinematic modeling follows the approach of *Delouis et al.* [2002]. The model consists of a single fault segment 31.5 km-long and 19.5 km-wide, subdivided into 273 subfaults measuring 1.5 km along strike and dip. The model area is purposely taken larger than the expected rupture surface in order to separate clearly the areas that slipped from those which did not. The strike and dip angles (325°, 55°) of the fault are kept fixed. Rupture initiation (model hypocenter) is located at 15.765°N, 61.502°W, and 10.5 km (0.5 km below the located hypocenter in Table 1 because of the model discretization). The continuous rupture is approximated by a summation of point sources evenly distributed on the fault plane, one at the center of each subfault. For each point source, a local source time function is defined, corresponding to the rate of seismic moment locally released, represented by a single isosceles triangular function of duration 0.4 s. For each of the 273 subfaults, the parameters to be inverted for are the slip onset time, the rake angle, and the amplitude of the triangular function. A non-linear inversion is performed with simulated annealing. Convergence is based on the simultaneous minimization of the root mean square (RMS) waveform misfits and of the total seismic moment. The RMS misfit error is the average of the normalized RMS errors of the individual data sets (teleseismic and strong motion), here equally weighted. Minimization of the total seismic moment is required to reduce spurious slip in the fault model. Since no geodetic data are available to help to stabilize the long wavelength characteristics of the slip model, a smoothing operator is applied to the slip distribution. We verified that the main features of the slip model described below are stable when the model discretization and data weighting is varied within reasonable limits.

[22] The slip model is characterized by two main slip zones, located 5 to 10 km to the SE and NW of the hypocenter (Figure 7a). Only a small portion of the total seismic moment was released in the hypocentral area. From the SE zone, slip propagated toward the surface with moderate amplitude (<1 m) implying a coseismic offset of 0.3 to 0.6 m of the seafloor along the Roseau fault. Larger slip occurred at depth with a maximum of 1.8 m in the SE slip zone at the southern tip of the Saintes Graben where two antithetic fault systems connect at depth. The northwestern patch ruptured the Roseau fault beneath the Saintes plateau attesting for the continuity of this fault along the western border of the plateau.

[23] The slip weighted average rupture velocity is 1.72 km/s. The two main zones ruptured approximately simultaneously, between 3 and 6 s after origin time, resulting in a single shaped pulse dominating the global source time function (Figure 7f). Slip direction indicates essentially normal faulting, with a small left-lateral component mainly observed at the SE slip zone. The waveform fit is shown in Figures 7c and 7e. More details on data sources, processing, and codes used are given in Appendix A.

[24] The slip model was retrieved through conjoint inversion of teleseismic and local data, using deterministic wave simulation in one-dimensional velocity structures. To validate our results, we have verified that propagation effects inadequately taken into account by this simplified structure have not affected the source model. The details of this validation, based on the Empirical Green Function (EGF) technique [*Hartzell*, 1978], can be found in Appendix A.

[25] The previous model determined by *Salichon et al.* [2009, Figure 4] has almost the same geometry (strike/dip/rake = 327/55/−89.8) and displays also slip zones on both sides of the hypocenter, with little slip at rupture initiation. However, their south-eastern rupture patch is much reduced in comparison to ours, and we found that slip propagated from this zone toward the surface, a characteristic absent from their model. In our case, a strong additional constraint is provided by the local strong motion records.

6. Stress Changes and Aftershocks

[26] Numerous recent studies have addressed the problem of stress transfer and interaction between large earthquakes, location of aftershocks sequences, and volcanic eruptions [see, e.g., *Nostro et al.*, 1997, 1998; *Harris*, 1998; *Stein*, 1999; *King and Cocco*, 2001; *Hill et al.*, 2002; *Steacy et al.*, 2005; *King*, 2007, references therein]. In view of its location in the heart of an active volcanic arc and of sustained monitoring for several years by a permanent seismic network, the Les Saintes earthquake offers a particularly interesting opportunity to investigate static stress interactions between faults and volcanoes in an oblique extensional regime.

[27] As customary, the coseismic ruptures are modeled as planar dislocations in an homogeneous elastic half-space [*Okada*, 1992]. We used the FARFALLE code of *Nostro et al.* [1997] that allows the use of a complex slip model to calculate the stress changes induced by the November 21 main shock. Static Coulomb stress changes (or variation in Coulomb Failure Function- CFF) caused by an earthquake on neighboring faults [*Harris*, 1998] are calculated by using the equation

$$\Delta CFF = \Delta\tau + \mu(\Delta\sigma_n + \Delta P), \quad (1)$$

where $\Delta\tau$ is the shear stress change computed in the direction of slip on the faults, $\Delta\sigma_n$ is the normal stress change (positive for extension), μ is the coefficient of friction and ΔP is the pore pressure change. A Coulomb stress increase favors failure of the faults. It is usually assumed [*Harris*, 1998; *King and Cocco*, 2001] that ΔP is proportional to the normal stress change ($\Delta P = -B\Delta\sigma_n$ where B is the Skempton parameter). According to this assumption, Coulomb stress changes are calculated through the relation

$$\Delta CFF = \Delta\tau + \mu'\Delta\sigma_n. \quad (2)$$

Beeler et al. [2000] however pointed out that the use of a constant apparent friction model instead of an isotropic homogeneous poro-elastic model, with ΔP equal to the volumetric (or mean) stress changes ($\Delta P = -B\Delta\sigma_{kk}/3$), may bias Coulomb stress calculations. We discuss the effects of changing the pore pressure model in Appendix B, and use the effective pore pressure model.

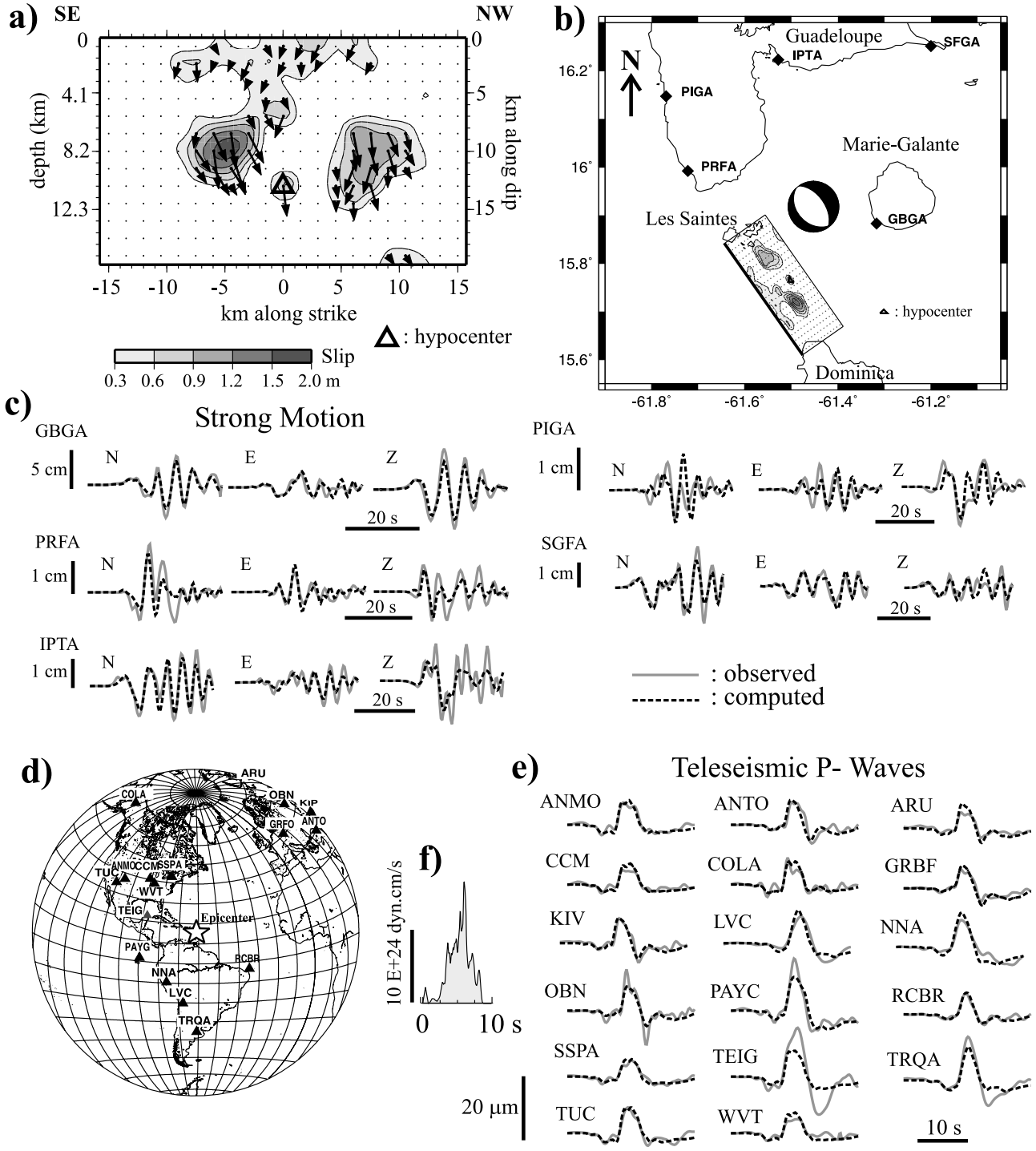

Figure 7. (a) Coseismic slip model for November 21, 2004 Saintes main shock (M_w = 6.3) from joint inversion of teleseismic and strong motion data. Black arrows indicate slip direction (amplitude proportional to slip). (b) Location of five strong motion stations used in this study. Also shown: focal mechanism of main shock (this study) and surface projection of fault slip model (plane striking N325°E, dipping 55°NE, heavy black line indicating intersection of plane with the free surface). (c) Waveform modeling of the strong motion records. (d) Location of broadband teleseismic stations used. Epicenter (star) at center. (e) Waveform modeling of the teleseismic P waves (SH waves not shown). (f) Overall source time function (seismic moment rate as a function of time).

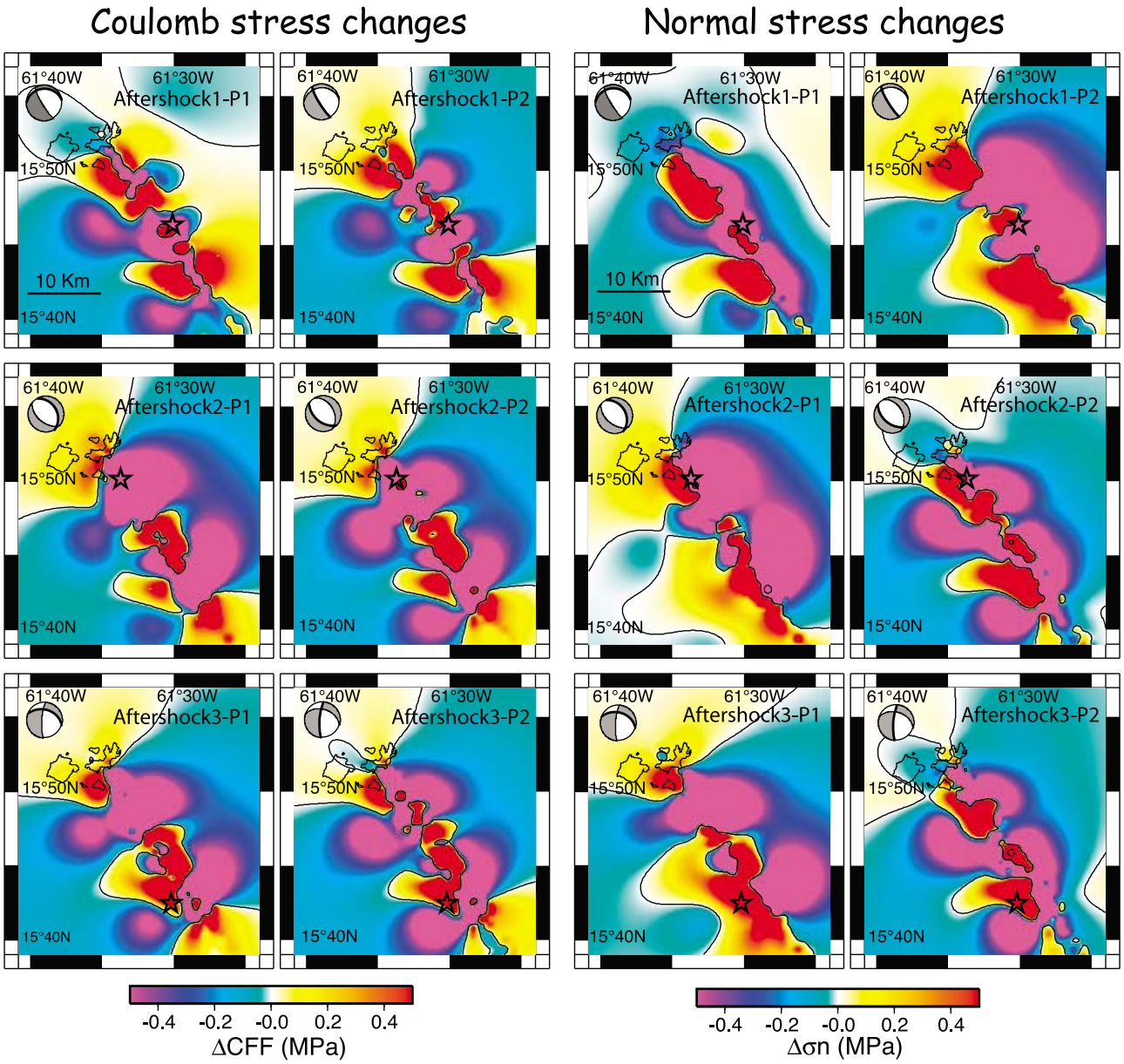

Figure 8a. Static Coulomb and normal stress transferred by main shock to fault planes of main aftershocks number 1 to 3 for which focal mechanism is available. Coulomb stress changes are calculated on both nodal planes P1 and P2, the plane on which stress is calculated being indicated in bold (see Table 1 for parameters). Black line: 0 contour. Blue colors: zones of stress decrease. Red colors: zone of stress increase. $\mu' = 0.4$, Lamé constants = 32 GPa. Maps are computed at hypocenter's depth.

[28] The Coulomb stress changes induced by a "master-fault" earthquake can be resolved on any "target" fault plane or in a pre-existing regional stress field. In the latter case, the failure planes are not specified and the stress changes are determined on planes optimally oriented for Coulomb failure. The plane orientations are determined from the total stress (regional stress field plus induced stress perturbation caused by the earthquake [*King and Cocco*, 2001]). Two conjugate planes are optimally oriented for stress, the Coulomb stress changes being identical on both planes, and a focal mechanism is associated to each plane. The Coulomb stress changes are sensitive to the regional stress direction [*King and Cocco*, 2001]. In the Les Saintes channel, the regional stress (N50 ± 15°E extension), is fairly well constrained by the fault geometry and the focal mechanisms. In Appendix B2, we modeled the effects of changing the direction and amplitude of regional stress and made all calculations with σ_3 horizontal, striking N50°E with an amplitude of 5 and 1 MPa (comparable to the stress drop calculated for the main shock dislocation: 0.65 MPa).

[29] We first calculated the coulomb and normal stress changes imparted by the main shock on the six main aftershock planes for which a focal mechanism is available (Figures 8a and 8b). We then calculated the stress changes on target faults with the same geometry as the master fault or along optimally oriented planes (Figure 9) to compare the stress

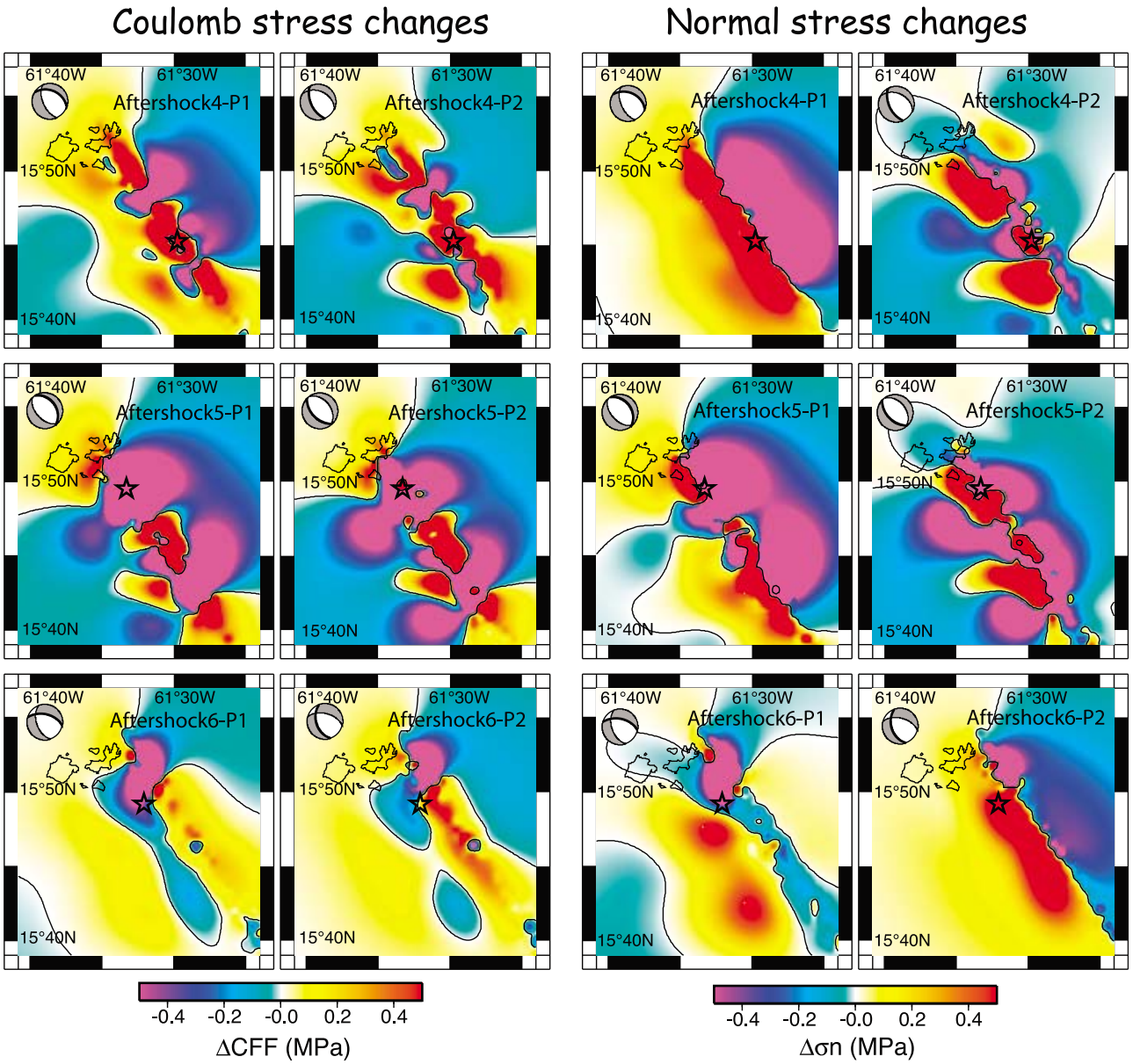

Figure 8b. Same as Figure 8a but for aftershocks number 4 to 6.

change pattern and the distribution of aftershocks. Finally we calculated the stress changes at earthquake hypocenters.

[30] For Figures 8a and 8b, the stress changes are calculated on both nodal planes of the six main aftershocks since we have no a-priori information on aftershock rupture dip. Each map is drawn at the aftershock's depth. The stress patterns are complex near the rupture with several small patches of stress increase or decrease within larger positive or negative lobes. Stress changes are larger than 0.4 MPa near the fault plane.

[31] Whatever the nodal plane considered, the aftershocks 3 and 4 occurred in zones of high Coulomb and normal stress increase (Figures 8a and 8b). Aftershocks 1 and 2 occurred in an area of Coulomb and normal stress decrease. Aftershock 1(and aftershock 2 by considering only the SW dipping plane) are however very close (less than 2 km far) to zones where the stress has strongly increased. Given our location errors, we cannot exclude that these events took place in an area of stress increase. By considering the SW dipping nodal plane, aftershock 5 occurred in a very small ($\approx$1 km^2) area of Coulomb stress increase but given the uncertainties on aftershock relocation, this could be questionable. By considering a rupture on a westward dipping plane, aftershock 6 occurred in an area of coulomb or normal stress increase.

[32] Only 50% (or 66% by considering aftershock 5) of the main aftershocks occurred in an area of stress increase. This result may be due to the local complexity of faults of the Les Saintes graben. *King* [2007] shows that calculating Coulomb stress changes onto a target fault plane is correct only if the average fault surface determined by focal mechanism represents the part of the fault where triggering has occurred.

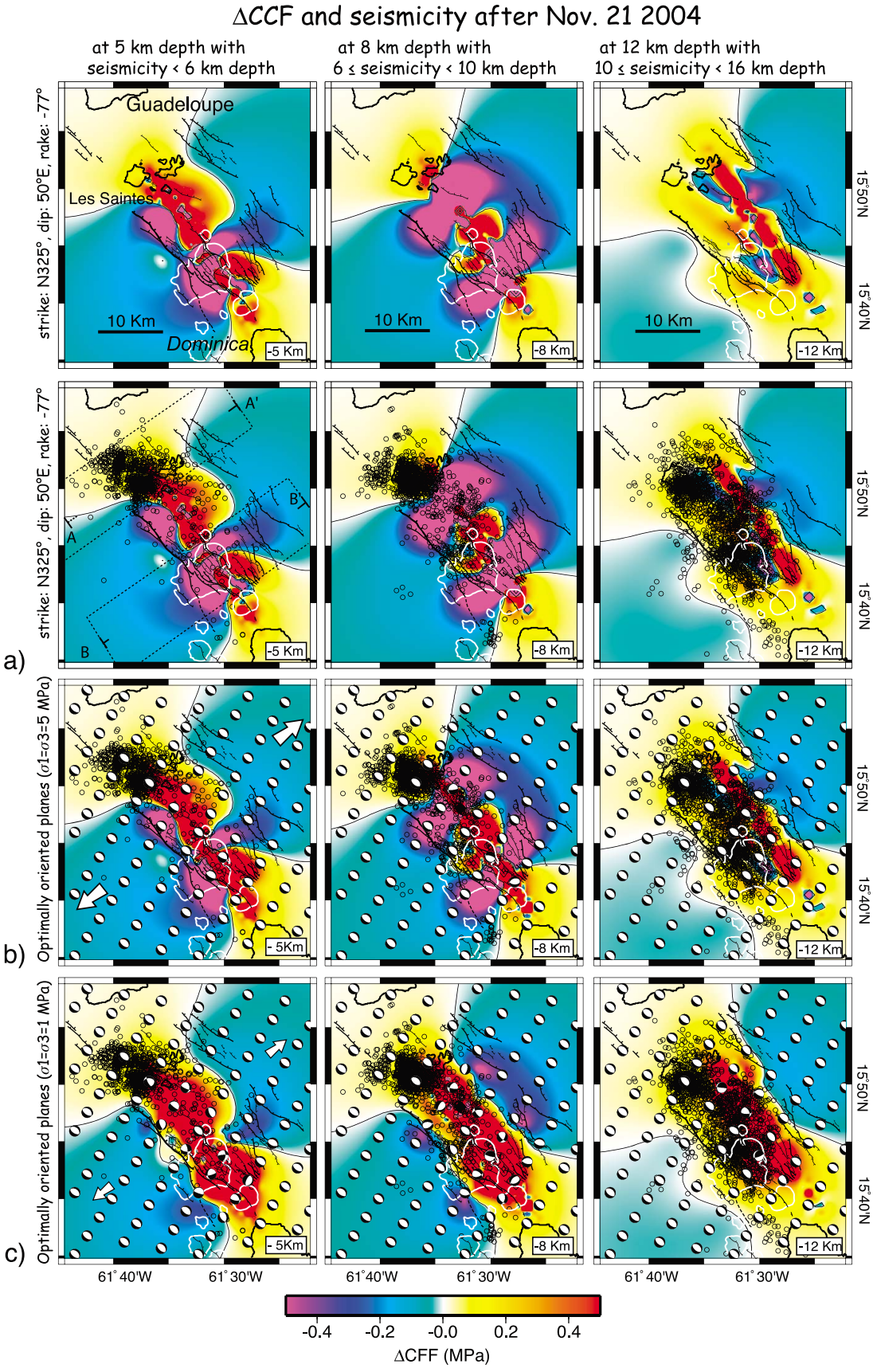
ΔCCF and seismicity after Nov. 21 2004
at 5 km depth with seismicity < 6 km depth
at 8 km depth with 6 ≤ seismicity < 10 km depth
at 12 km depth with 10 ≤ seismicity < 16 km depth
strike: N325°, dip: 50°E, rake: -77°
Guadeloupe
Les Saintes
Dominica
10 Km
-5 Km
-8 Km
-12 Km
A
A'
B
B'
a)
Optimally oriented planes (σ1=σ3=5 MPa)
b)
Optimally oriented planes (σ1=σ3=1 MPa)
c)
15°50'N
15°40'N
61° 40'W
61° 30'W
-0.4
-0.2
-0.0
0.2
0.4
ΔCFF (MPa)

Figure 9

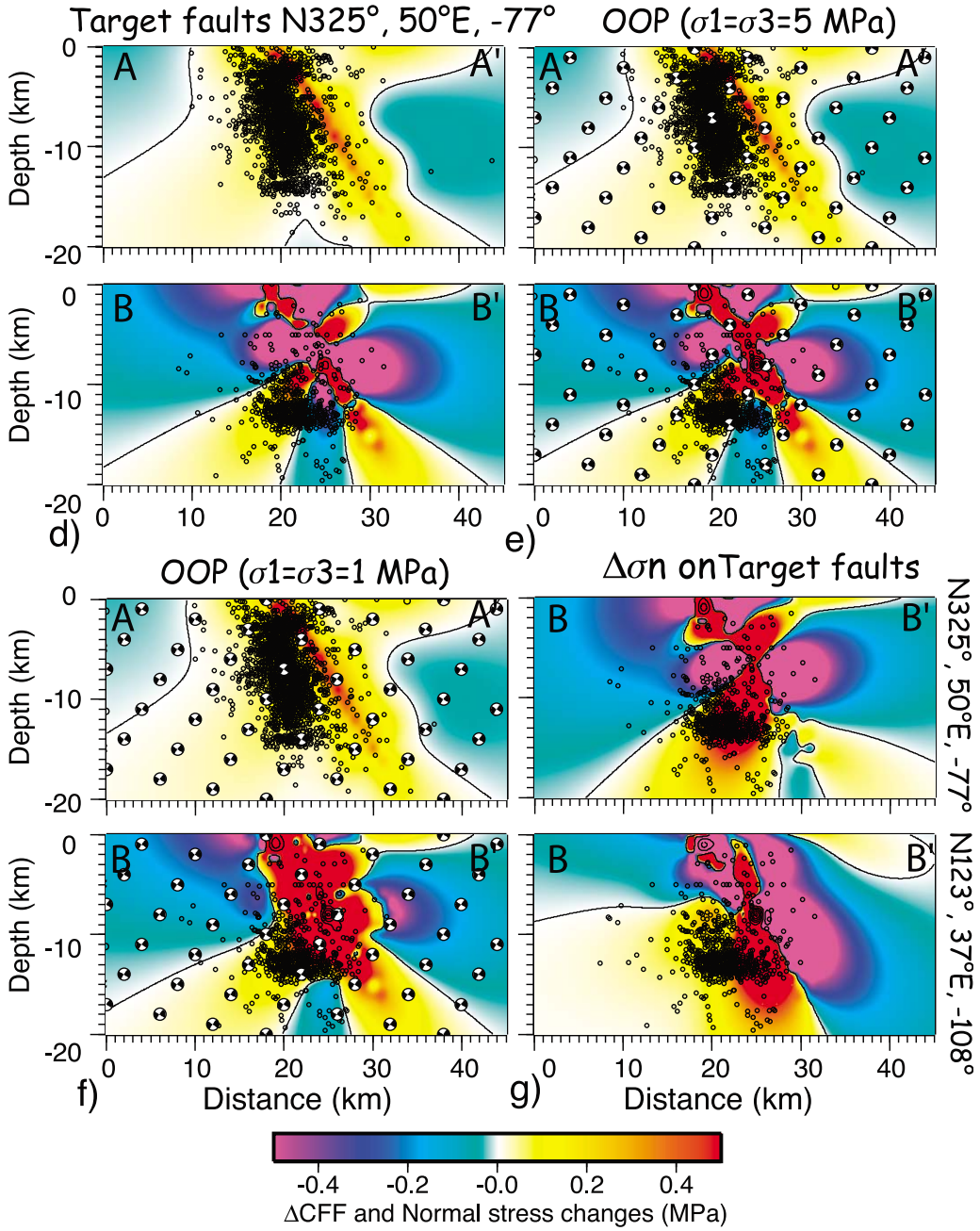

Figure 9. (continued)

Figure 9. (a) Coulomb stress transferred by November 21, 2004 earthquake on faults having same geometry as main dislocations (Strike: N325°E, dip: 50°E, rake: −77°) in maps at 5 (middle of dislocation), 8 and 12 km depth (beneath dislocation) without and with epicenters. Epicenters of aftershocks with depths < 6 km, between 6 and 10 km, and between 10 and 16 km are projected on maps at 5, 8, and 12 km depth respectively. $\mu' = 0.4$. Lamé constants are 32 Gpa. Dashed boxes: cross-sections of seismicity showed in Figures 9d–9g. Locations of vertical cross-sections AA′ and BB′ and submarine volcanoes (contoured in white) are indicated in Figure 9a. Red colors: areas of stress increase. Blue colors: areas of stress decrease. (b and c) Coulomb stress changes calculated on optimally oriented planes (OOP) in extensional regional stress field with σ_3 (white arrows) horizontal, oriented N50°E, and σ_1 vertical. $|\sigma_3| = |\sigma_1| = 1$ MPa and 5 MPa, for Figures 9c and 9b, respectively. Focal mechanisms show motion on SE-dipping OOP. (d) As in Figure 9a, along AA′ and BB′ vertical cross-sections (see location on Figures 9a and 9c) with aftershocks located in 10 km-wide vertical bands. (e and f) As in Figures 9b and 9c, along vertical cross-section AA′ and BB′. (g) Normal stress changes induced by main shock on BB′ vertical cross-section on fault having same geometry as main dislocations and on east-dipping plane, respectively. Constants as in Figure 9a. Seismicity as in Figure 9d.

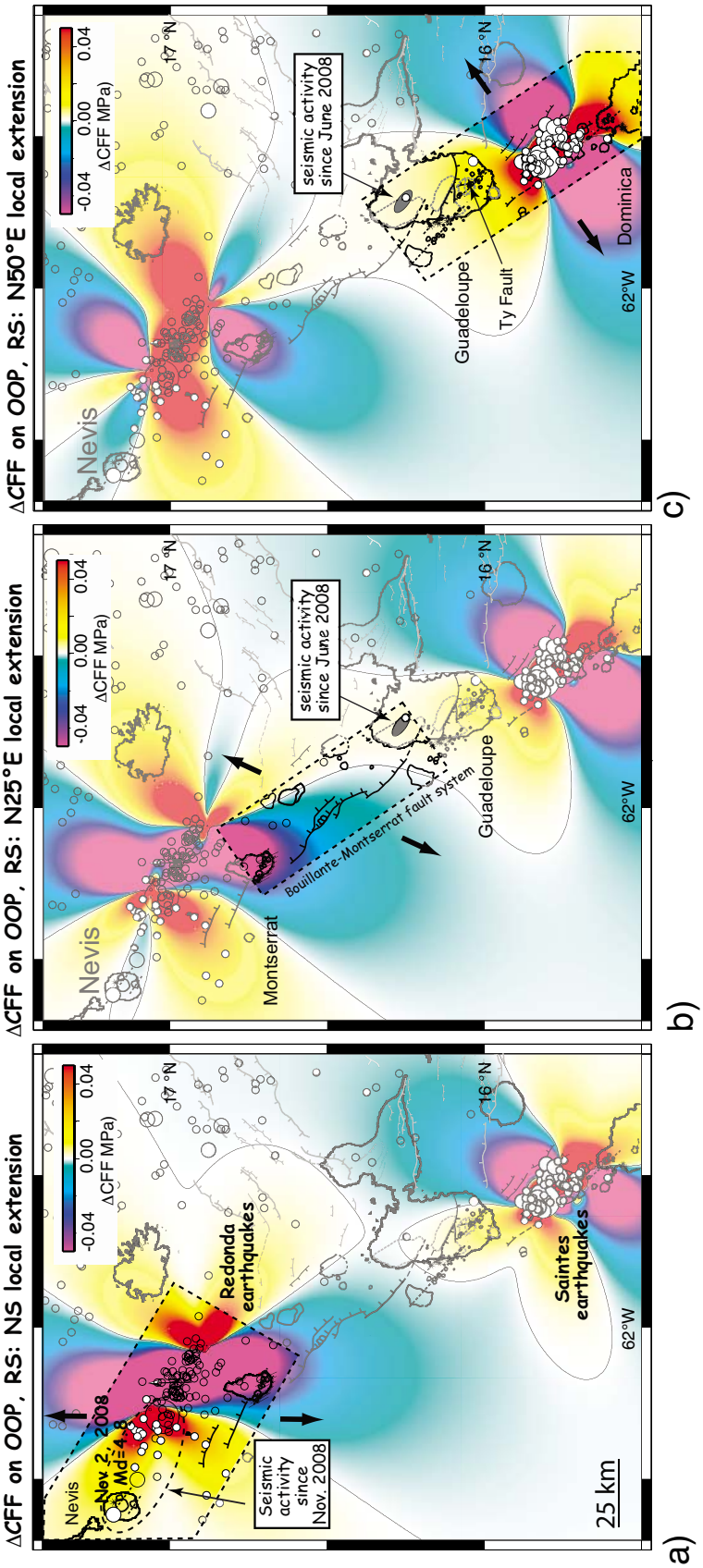
ΔCFF on OOP, RS: NS local extension
ΔCFF on OOP, RS: N25°E local extension
ΔCFF on OOP, RS: N50°E local extension
-0.04 0.00 0.04
ΔCFF MPa)
17 °N
16 °N
62°W
Nevis
Nov. 2, 2008 Md=4.8
Seismic activity since Nov. 2008
Redonda earthquakes
Saintes earthquakes
25 km
Montserrat
Bouillante-Montserrat fault system
Guadeloupe
seismic activity since June 2008
Ty Fault
Dominica
a)
b)
c)

Figure 10

[33] In Figure 9, we show the Coulomb stress changes induced by the main shock either on faults having the same geometry as the master-fault (Figures 9a and 9d), or along optimally oriented planes with a regional stress having an amplitude of 5 MPa (Figures 9b and 9e) and 1 MPa (Figures 9c and 9f). We also calculated the Coulomb stress changes on faults antithetic to the Roseau fault and verified that the stress change patterns remain roughly the same.

[34] The coulomb stress change patterns account well for the distribution of aftershocks, the majority of which are located in red lobes where stress increased. By calculating the stress changes at the 3977 hypocenters either on faults having the same geometry or along optimally oriented planes, we find that 75% and 94% (81% for a regional stress of 5 MPa) of aftershocks are located in an area of stress increase, respectively. Both models show roughly the same pattern of Coulomb stress change. The modeled focal mechanisms agree with both the focal mechanisms of the main shocks and the average strike of the faults.

[35] Most of aftershocks occurred beneath the Les Saintes insular shelf, within a steep east-dipping zone where the Coulomb stress increased by more than 0.4 MPa. These aftershocks cluster along a southward dipping plane (cross-sections AA′ on Figure 9). This suggests that rupture on the Roseau fault may have triggered aftershocks on a northernmost fault segment crossing Les Saintes insular shelf (Figure 2). The absence of aftershocks in the eastern part of the system, along the Marigot, Rodrigues, Souffleur and on the northeast-dipping faults cutting the eastern Saintes shelf, is consistent with a Coulomb stress decrease (0.3 MPa on average). However, the fact that few aftershocks occurred south of the Roseau fault southern tip implies that the Les Saintes Channel fault system as such terminates at the Colibri volcano. That several events occurred Northwest of the tip of Dominica is nevertheless not at odds with the stress increase there. This area appears to be crosscut by another segment of the inner-arc en echelon fault system (Figure 1b).

[36] The redistribution of stress account for the seismicity cluster at the base of the rupture between 11 and 15 km (cross-sections BB′ on Figures 9e and 9f), where the Coulomb stress increase was more than 0.4 MPa. These deep aftershocks are not likely promoted by fluid flows related to volcanic processes. We calculate that the moment release doubles as average fault dimension double with scaling corresponding to a b-value of 1 what is typical of tectonic deformation [*Amelung and King*, 1997] (Figure 4a, inset). Moment release independent of fault dimension is characteristic of swarm where fluids are involved. The deep aftershocks are likely promoted by the static stress increase at the down-dip tip of a rupture that stopped short of cutting the base of the seismogenic zone.

[37] By calculating the shear and normal stress changes associated with the main shock on faults having the same geometry and along optimally oriented planes, we show that the normal stress change pattern explains well the distribution of these deeper aftershocks (Figure 9g), particularly when calculated on east-dipping planes. When calculating the normal stress changes at earthquake hypocenters for east-dipping optimally oriented planes, 91% (85% for a regional stress of 5 MPa) of the aftershocks fall where the normal stress increased. The deeper aftershocks occurred in a zone where the normal stress increased by more than 0.4 MPa and thus could have been triggered by unclamping of faults beneath the rupture zone.

[38] Our results show that most aftershocks were probably promoted by an increase of static stress induced by the main shock. Some may however have also been triggered by fluid flow induced by an increase of extensional stress [*Noir et al.*, 1997]. *Miller et al.* [2004] inferred that pressurized fluids or gas propagating through the damage zones created by the main shock might promote aftershocks of large earthquakes. Evidence for fluid discharge is presented by *Bazin et al.* [2010]. A few minutes after the February 14th 2005 aftershock, Patrick Bellenus, City Hall employee of Terre-de haut, and other residents of this island, observed a several hundred meters long white patch on the surface of the sea. This patch was visible long enough for photographs to be taken (Figure 5e, location Figure 2b inset). Some inhabitants described intense boiling associated with vapor (see details in Appendix C). This phenomenon could be related to submarine venting of gas or fluids, perhaps not surprising since the earthquakes took place near the axis of the active volcanic arc.

7. Stress Changes on the Inner Arc En Echelon Fault System

[39] At the scale of the arc, we modeled the stress changes induced both by the 21 November 2004, Les Saintes, and 16 March 1985 Redonda earthquakes on the Bouillante-Montserrat segment, between the epicenters of the two events (Figure 10b). The Redonda earthquake was studied by *Girardin et al.* [1991]. The 1985–1986 and 2004–2008 seismic crisis show several similarities. The two main shocks are intraplate events that ruptured faults of the inner system parallel to the arc. The depth estimated for the March 16, 1985 earthquake ranges between 7 and 11 km. More than 3000 aftershocks with magnitudes between 2 and 4.5 were recorded by the regional network in the first 3 weeks. As in 2004, the aftershock activity lasted many months and the main aftershock (M_s = 5.1) occurred months after the main shock (February 12, 1986). The aftershock distribution suggests rupture of a fault striking ≈N130°E, about 30 km-long

Figure 10. Coulomb stress changes induced on optimally oriented planes (neighboring faults) by M_w = 6.3, 16/03/1985 and 21/11/2004, earthquakes at 5 km depth. (a) In pre-existing regional stress, with σ_3 horizontal, NS-striking, consistent with focal mechanism of March 16, 1985 earthquake. (b) In pre-existing regional stress with σ_3 horizontal and N25°E-striking, consistent with volcanic domes alignments and fault geometry. (c) In pre-existing regional stress with σ_3 horizontal and N50° E-striking, consistent with fault geometry and focal mechanisms. Magnitude of regional stress is taken to be 2 MPa (see text). The 16/03/1985 earthquake model is N132°E-striking, 80°N dipping, 30 km-long, 15 km-wide, pure left-lateral strike-slip dislocation of 0.3m centered at 62.173°W, 16.965°N. Faults and seismicity as in Figure 1b with earthquakes postdating the November 21, 2004 shock in white. Gray ellipse: area of Pointe-Noire earthquakes in northern Basse-Terre.

and 15 km-wide [*Girardin et al.*, 1991]. The average slip was estimated to be ≈0.3 m. However, instead of primarily normal faulting as in Les Saintes, the focal mechanism from the Harvard database [*Dziewonski et al.*, 2000] shows pure left lateral strike-slip motion on a N132°E-striking plane. These parameters were used to model the 16 March 1985 rupture as a 30 km-long, 15 km-wide dislocation with 0.3 m of pure strike slip in a N132°E azimuth. Near Montserrat, the local extension is about N25°E (25° more northerly than in Les Saintes), if taken perpendicular to the en echelon normal faults and alignments of volcanic domes [*Feuillet et al.*, 2010]. We calculate the stress changes along the Bouillante-Montserrat fault system in a N25°E extensional regional stress field (Figure 10b). The amplitude of this regional stress is set to 2 MPa, close to the stress drop calculated for the modeled 16 March 1985 rupture. The results are not very sensitive to the amplitude of regional stress far from the faults [e.g., *King and Cocco*, 2001]. The modeling shows that the 1985 earthquake decreased the Coulomb stress along the north part the Bouillante-Montserrat fault system, while the 2004 event increased it slightly along the southern part. This may explain why no earthquake, even with a small magnitude, was recorded along these faults since the installation of the regional seismic network at the beginning of eighties [*Feuillet*, 2000] (Figure 1b). A coulomb stress decrease promotes a reduction of the seismic activity by discouraging failure [*Stein*, 1999]. By contrast, the seismic activity increased significantly in Northern Basse-Terre with the occurrence of several $M > 3$ earthquakes in 2008, in an area where only few very small events were recorded in the last thirty years. These earthquakes are concentrated in an elongated N-E-trending zone at the southern tip of the Bouillante-Montserrat fault zone.

[40] The 2004 earthquake increased the Coulomb stress north of Les Saintes and could have brought regional faults closer to failure (Figure 10c). At least one branch of the en echelon fault system appears to continue toward the southern tip of Basse-Terre (Figures 1b and 2). Given its length, rupture of this fault could produce an earthquake with a magnitude comparable to that of the November 21, 2004 event. The Ty fault, which crosscuts the summit of Guadeloupe's most recent volcanic complex (<200 ka), down-dropping the eastern half of the Soufrière dome [*Feuillet et al.*, 2002], strikes roughly parallel to the Roseau fault, and thus likely belongs to the "inner arc fault system". The 2004 stress increase in the area, while smaller than between Les Saintes and Basse-Terre, may also have contributed to advance failure of this latter fault, which in turn would raise the local level of volcanic hazard.

[41] Finally, it is also noteworthy that several fairly strong shallow earthquakes occurred in November 2008 north of Montserrat, four years after the November 21, 2004 shock (Figure 10a). The largest ($M \approx 4.8$) struck Nevis on November 2. It was followed by several aftershocks along a NW-SE trending zone, on the westward continuation of the 1985 rupture, suggesting rupture of the same en echelon fault system. The 1985 earthquake had increased the Coulomb stress by more than 0.05 MPa in this area, twenty years before. Perhaps the additional occurrence of the 2004 earthquake, farther south, contributed to finally promote the strong resurgence of seismic activity in Montserrat in late 2008. The 2008 seismic activity has preceded a strong increase of volcanic activity in December 2008 that ended with the dome collapse in February 2010 (see reports on Soufriere Hills volcanic activity on http://www.mvo.ms/).

8. Consequences of the 21/11/2004 Earthquake on Volcanic Activity

[42] The 2004 earthquake occurred along the inner arc, which is where the active volcanoes are located. Intensified monitoring of the Soufriere volcano was performed by the observatory staff for many weeks after the earthquake. The chemical composition of geothermal sources around the volcano, in particular, was measured almost daily. To this day however, no anomalous seismic or geochemical signal was detected. The seismic and fumarolic activity near and on the Soufrière dome appears to have remained constant with the exception of the large landslides triggered by coseismic shaking on its southern flank (see more details on interactions between earthquakes and volcanoes from *Feuillet et al.* [2011]).

[43] The only notable consequence of the 2004 events took place in the southern part of Dominica where the Boiling Lake is reported to have drained out completely following the November 21st shock (http://www.natureisland.com/BoilingLake.html [*Lindsay et al.*, 2005; *Fournier et al.*, 2009]). This lake (15°19′6″N, 61°17′38″W), located in southern Dominica, close to the Valley of Desolation (Figure 11a), fills explosion craters due to phreatic eruptions, the last of which occurred in January 1880 and July 1997. The valley is a site of intense geothermal activity with numerous hot springs, bubbling pools and fumaroles. The Boiling Lake is an almost circular water-body, with a diameter of ≈80 m. It is 10 to 15 m deep, with a temperature ranging between 80 and 90°C. The behavior of the lake level has been stable over the last 150 years. A few short-term fluctuations with drop of the lake level were however reported at end of the 19th century (in 1876, 1887, 1900, 1901), in 1971 and 1988 [*Lindsay et al.*, 2005] and references therein. The last such events, described below, occurred in 2004 and 2005 (Figures 11b and 12).

[44] During heavy rainfall, the lake inflow and outflow increase, promoting a decrease of the lake temperature by a few degrees. No particular meteorological phenomena was reported, however, during the 2004 and 2005 events [*Fournier et al.*, 2009].

[45] On 25 December 2004, about one month after the 21st November earthquake, tourists discovered that the lake was empty (Figure 12a). It was subsequently monitored by the Dominican forestry division for 4 months, until it regained its usual level. On December 28, 2004, the water level had dropped by 10 to 12 m. The lake began to refill in mid-January (Figure 12b). On January 28, 2005, it was about 3 m below its normal level (Figure 12c). On February 11, it was still 2 m below normal and the water temperature was only 20°C (Figure 12d). By February 14, the lake was completely full, but was not boiling. On February 14, the main aftershock occurred and the level of the lake dropped again. On February 21, it was 4.5 m below normal and the water temperature was 18°C (Figure 12e). On March 7, the lake was almost empty again but with more intense bubbling (Figure 12f). Between March 18 and 31, the level of the lake was still low (Figures 12g and 12h) but on April 13, it was

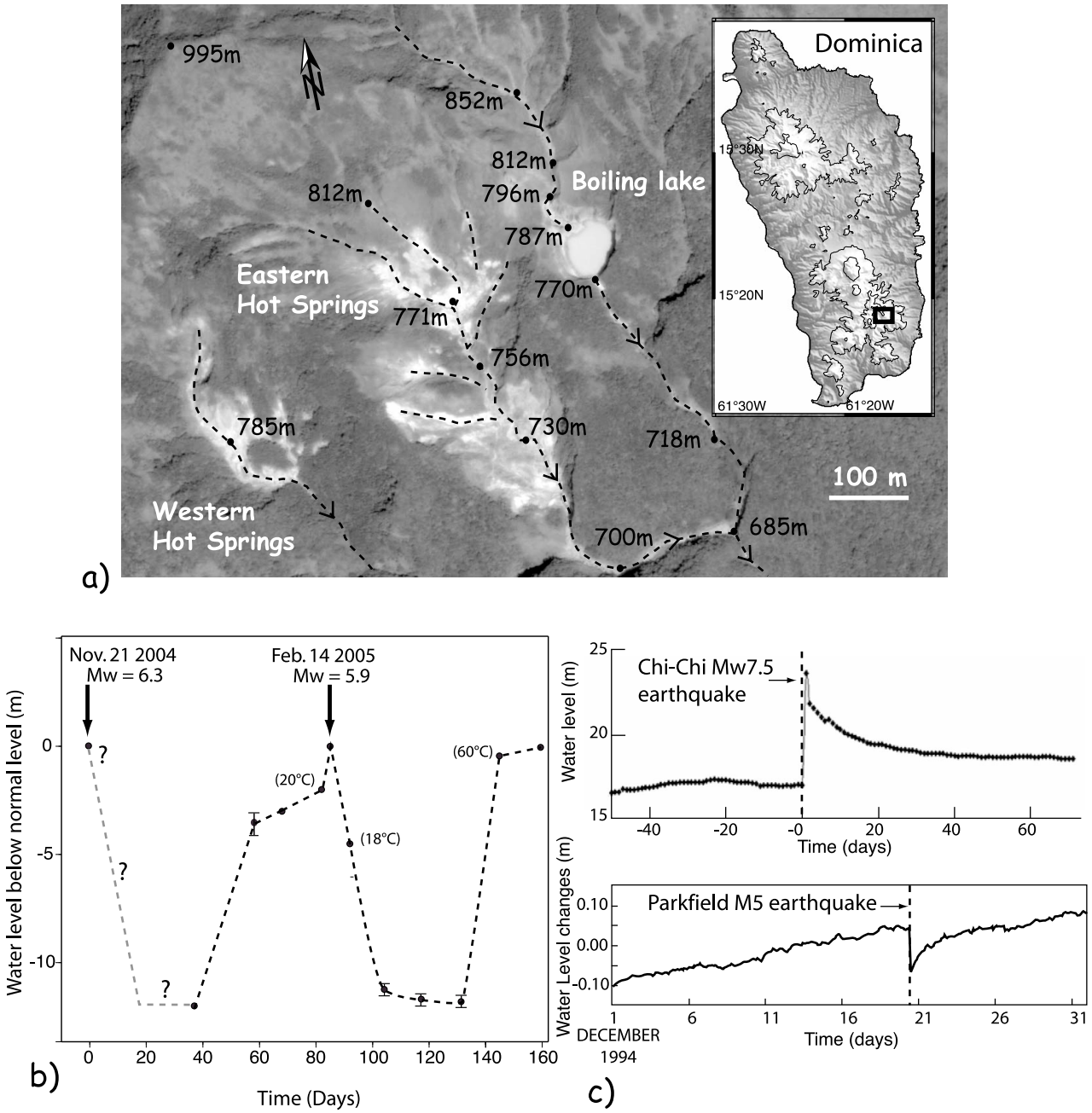

Figure 11. (a) Google Earth satellite view and map of Boiling Lake and Valley of Desolation in Dominica. Topography from SRTM3. Google Earth imagery © Google Inc. Used with permission. (b) Variations of water level of Boiling Lake, with temperature in °C when measured. Data from Dominican Forestry & Wildlife Division (http://www.natureisland.com/BoilingLake.html). (c) Example of water level changes recorded in wells after large or moderate earthquakes (Chi-chi, Taiwan, *Chia et al.* [2001]; Parkfield, USA, *Quilty and Roeloffs* [1997]).

almost completely full (0.5 m below normal) and the water temperature at the edge had reached 60°C (Figure 12i). By late April, the lake was boiling again. Photograph on Figure 12j taken on June 23, 2005, shows the lake at its usual level with its off-centered vapor plume.

9. Stress Changes at Boiling Lake

[46] Earthquakes are often associated to hydrological effects, such as increase in spring or river discharge or groundwater level changes in wells [*Muir-Wood and King*, 1993]. Several physical models have been proposed to explain these effects. *Muir-Wood and King* [1993] have shown that the earthquake-induced static strain changes within few source dimensions of the epicenter perturb the effective porosity in important portions of the brittle crust by closing or opening fracture systems extending to considerable depths. When cracks are closing, the water is expelled. When cracks are opening, they are filled from the water

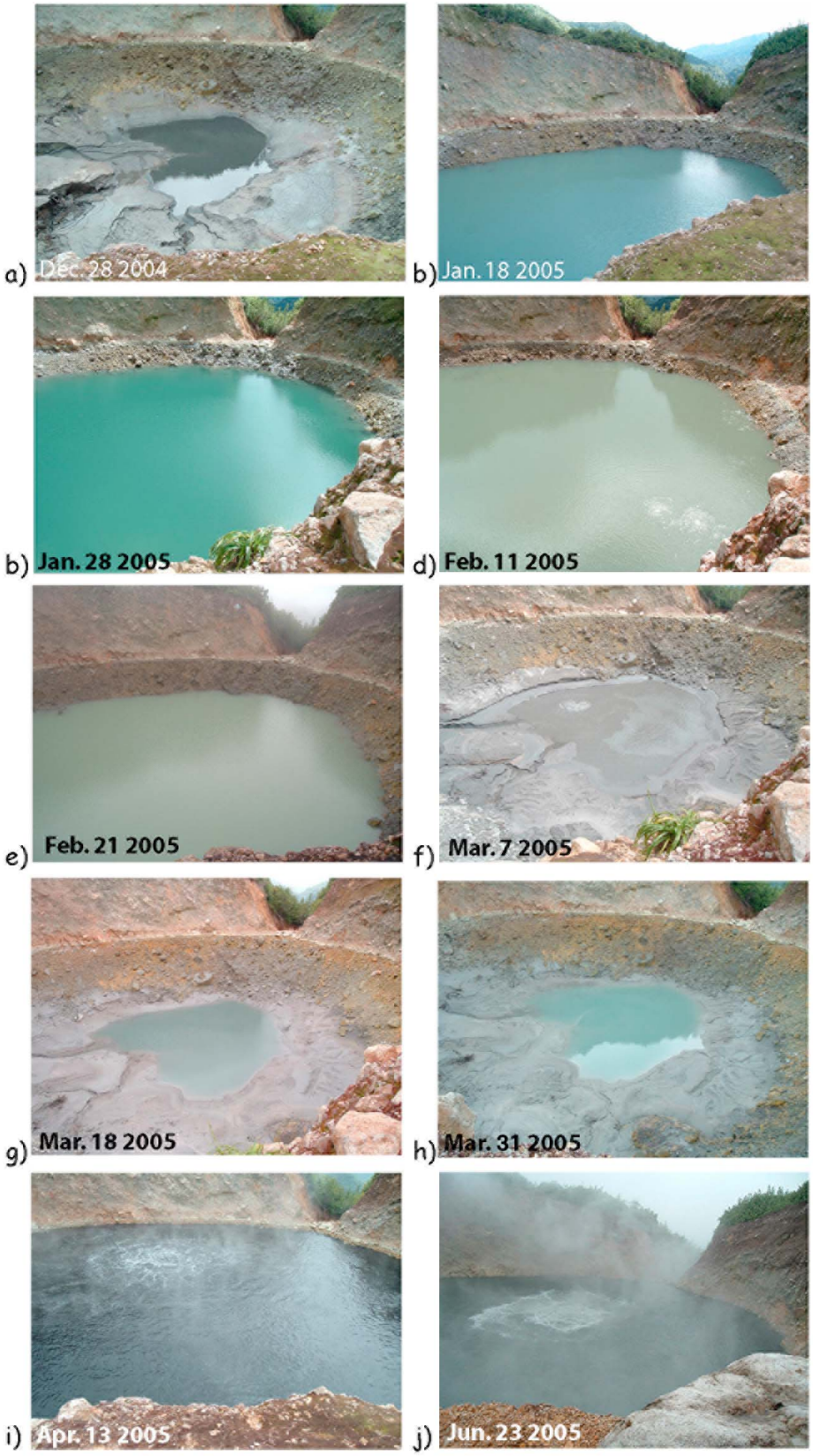

Figure 12. Photographs of Boiling Lake taken by the Dominican Forestry & Wildlife Division (Arlington James) between December 2004 and June 2005.

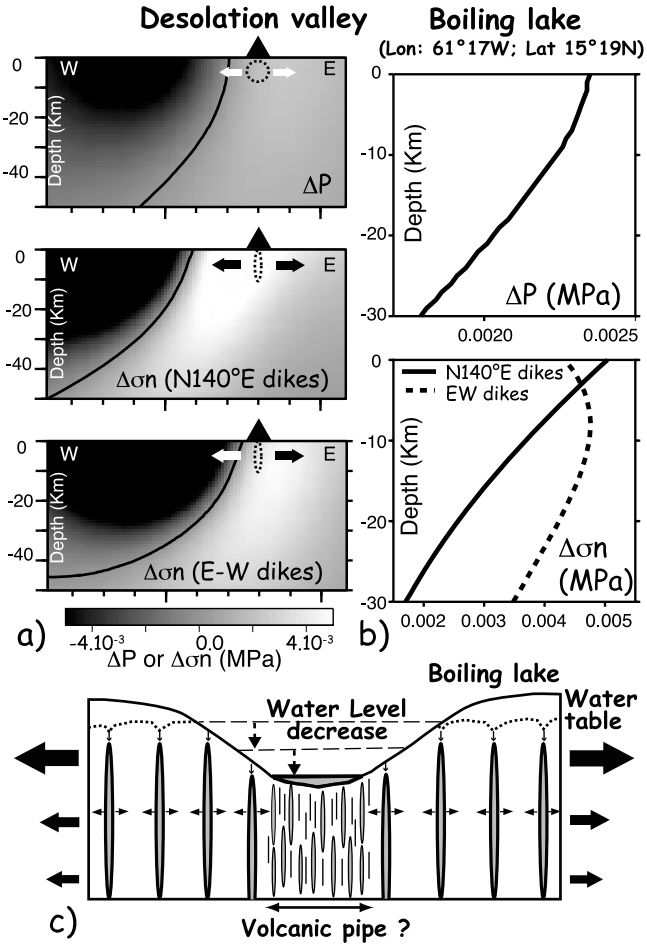

Figure 13. Pressure (ΔP) and horizontal normal changes ($\Delta\sigma_n$ induced by the November 21, 2004 earthquake (a) along E-W cross-section under Boiling Lake in Southern Dominica (Arrows: expansion), (b) along a vertical profile under Boiling Lake. (c) Sketch adapted from [*Muir-Wood and King*, 1993] for Boiling Lake, showing possible effect of extensional strain on lake water level: cracks open and water is drawn in. In gray: open fissures. Dashed line, water table level.

table implying water level drops in wells. The static strain changes pattern and then the induced hydrological effects depend on fault geometry. Sustained water level changes in wells also occur in response to seismic oscillations from distant events. The signal can be modeled by diffusion of a coseismic pore pressure step near the wells that may be promoted by unclogging of narrow fractures, escape of gas bubbles from the aquifer or liquefaction [e.g., *Brodsky et al.*, 2003; *Roeloffs et al.*, 2003].

[47] The water level changes observed at Boiling Lake (Figure 11b) resemble others elsewhere, particularly in wells after moderate or large earthquakes [*Chia et al.*, 2001; *Quilty and Roeloffs*, 1997] (Figure 11c). We have no information on lake level just after the November 21 main shock but following the February 14 main aftershock, the lake was emptied in two weeks and refilled progressively in the following months. These timescales (rapid draining and longer-time refilling) are typical of earthquakes hydrological signatures [*Muir-Wood and King*, 1993].

[48] The lake being only 50 km far from the 2004 and 2005 earthquake epicenters, its water level changes could be related to earthquake induced static stress changes [*Muir-Wood and King*, 1993]. We calculated the horizontal normal stress changes on dikes parallel to inner and outer arc faults (N140°E and E–W) as well as the pressure changes induced by the November 21 and February 14 earthquakes at Boiling Lake. The modeling shows that the 2004 earthquake and its largest aftershocks induced a horizontal normal stress increase and a pressure decrease, around the Boiling Lake, with larger values near the surface (Figures 13a and 13b). Such dilation (or expansion) induced at the tips of the 2004 and 2005 ruptures plane may have contributed to open cracks and diminish water inflow, drying-up springs and lakes in the Desolation valley (Figure 13c). In the absence of information on aquifer and plumbing system geometry, we cannot model the variations of the lake level and discriminate between mechanisms but we show that the drop of the lake level is compatible with a extensional coseismic volume strain in this region. Other processes due to seismic waves propagation or ground shaking may have occurred however in this complex hydrothermal system including the effects of vapor and bubbles in a highly fractured conduit.

10. Conclusions

[49] Seismic and bathymetric data, the distribution of damage and landslides, and the regional kinematics single out the Roseau normal fault as the most likely source of the November 21, 2004, $M = 6.3$ Les Saintes earthquake within the inner arc fault system. Seismological data shows that the rupture initiated at 10 km-depth and that the main slip occurred on two $\approx 5 \times 5$ km^2 patches. The February 14, 2005 main aftershock occurred close to the northernmost slip zone. Following the slip model, the rupture had reached the seafloor in agreement with occurrence of a tsunami [*Le Friant et al.*, 2008]. The expected coseismic offset is at most 0.6 m at the surface and occurred where the Roseau scarp is the highest. This may suggest that the 2004 earthquake could be characteristic with similar slip functions from one earthquake to another [*Sieh*, 1996]. Coulomb modeling, based on the slip model, accounts for the aftershock distribution and suggested that most aftershocks were triggered by a Coulomb static stress increase induced by the main shock.

[50] The 2004 earthquake ruptured a segment of a large en echelon fault system along the volcanic arc and raised the Coulomb stress north of Les Saintes. This may have brought regional faults closer to failure near to the densely populated area of southern Basse-Terre (Guadeloupe), and the Soufrière volcano, suggesting an increase of both the seismic and volcanic hazard in this region. Intensified monitoring of the Soufrière volcano was performed after the earthquake. No increase in volcanic or geothermal activity at Guadeloupe's Soufrière volcano has yet been observed [*Feuillet et al.*, 2011]. In contrast, the 2004 earthquake had a dramatic effect on the hydrothermal zone of southern Dominica, which lies farther away to the south. The Boiling Lake which is 10 to 15 m-deep rapidly drained twice immediately following the 2004 event and its main aftershock. We have calculated that

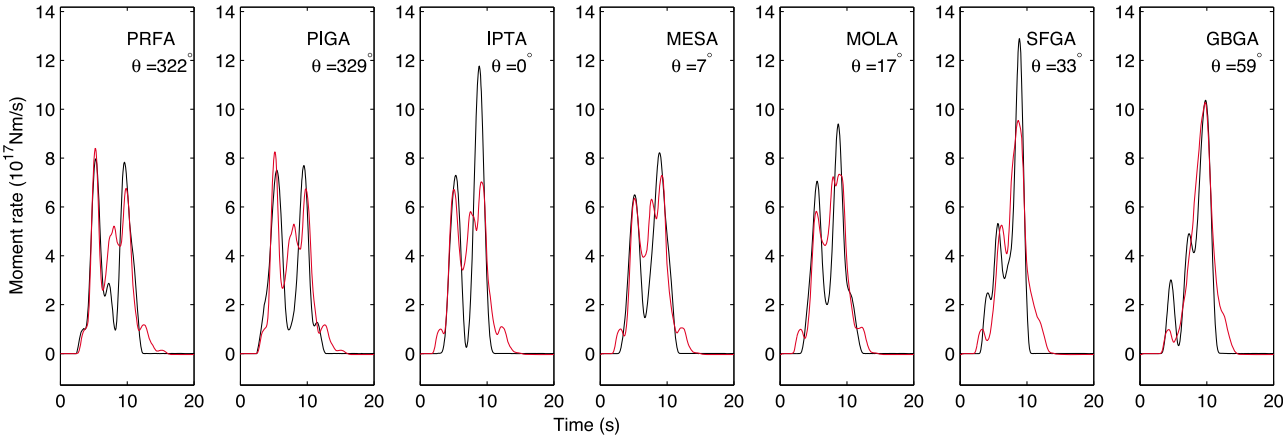

Figure A1. Comparison between observed and synthetic RSTFs (Relative Source Time Function). Observed RSTFs (black) are retrieved from deconvolving EGF signal from main shock signal, while synthetic RSTFs (red) are computed from Saintes earthquake source model (Figure 7a). Both observed and synthetic RSTFs are smoothed at 1s. Name and north azimuth of each station are shown in each figure. Location of 5 RAP stations PRFA, PIGA, IPTA, SFGA, GBGA in Figure 7b), while MESA and MOLA are located between IPTA and SFGA, slightly farther North in Guadeloupe Island.

the earthquake has promoted a volumetric strain expansion around the lake, at the southern tip of the rupture. This has contributed to increase the effective porosity by opening cracks causing the lake to drain rapidly and then later slowly refilling.

Appendix A: Slip Modeling

A1. Data Processing, Data Source, and Synthetic Seismograms Generation in the Slip Inversion of the Main Shock

[51] Broadband teleseismic seismograms (stations shown in Figure 7d) were retrieved from the IRIS data center (http://www.iris.edu/wilber). The strong motion records at stations GBGA, PRFA, IPTA, PIGA, and SFGA (Figure 7b) were obtained from the French accelerometric network (RAP, http://www-rap.obs.ujf-grenoble.fr). Processing of the teleseismic records includes deconvolution from the instrument response, integration to obtain displacement, windowing around the P (vertical) and SH wave train, equalization to a common magnification and epicentral distance, and bandpass filtering between 0.01 and 0.8 Hz for the P waves and 0.01 to 0.4 Hz for the S waves. SH waves, included in the analysis but characterized by a lower frequency content in comparison to the P waves, are not shown in Figure 7. The strong motion records were twice integrated to obtain displacement seismograms and bandpass filtered between 0.03 and 0.35 Hz to reduce both the low-frequency noise produced by the integration process and the high-frequency content related to the complexity of the real earth structure.

[52] Synthetic seismograms at local distances (strong motion data) are computed using the discrete wave number method of *Bouchon* [1981] designed for one-dimensional velocity models. A specific layered velocity model is used for each of the five strong motion stations. Velocity models were optimized by modeling the waveforms of the aftershock 14/12/2004 21:29 [UTC], 15.77°N, 61.49°W, depth 11 km, Mb 4.6 [*Bertil et al.*, 2005] located within a few km from the main shock. Synthetic seismograms at teleseismic stations were generated using ray-theory approximation and the approach by *Nabelek* [1984].

A2. Validation of the Slip Model by Empirical Green Function Approach

[53] The EGF (Empirical Green Function) is an earthquake similar to (in terms of location and focal mechanism) but smaller than the main shock. At each station, deconvolving the EGF signals from the main shock signals gives the source time function relative to this station, thus called Relative Source Time Function (RSTF). These RSTFs, which are closely related to the spatiotemporal source properties, are obtained without making assumptions on Earth propagation because this term is present both in the EGF and main shock signals and thus vanishes during deconvolution. The deconvolution process can be made more stable by the introduction of physical constraints on the RSTF (positivity and causality in particular) and we follow here the methodology proposed by *Vallée* [2004].

[54] The abundant seismicity after the main shock gives us the opportunity to check several EGFs in order to verify that the RSTFs are not dependent on the choice of the EGF. This is important in the case of the Saintes earthquake, because RAP stations are close to the earthquake, which could limit the precision of the EGF approach. Practically, we have used the EGF technique with 4 aftershocks (2004/11/21 18:53; 2004/11/21 22:56; 2004/11/26 05:05; 2004/12/14 21:29) and have verified the compatibility of the obtained RSTFs, which confirms the suitability of the EGF approach. We present in Figure A1 the RSTFs obtained (called observed RSTFs) for 7 stations of the RAP network.

[55] As expected for an extended source, the RSTFs differ from station to station and differ also from the absolute source time function presented in Figure 7f). These changes in the shape of the RSTFs are simply related to the rupture process characteristics (slip location, rupture velocity). We

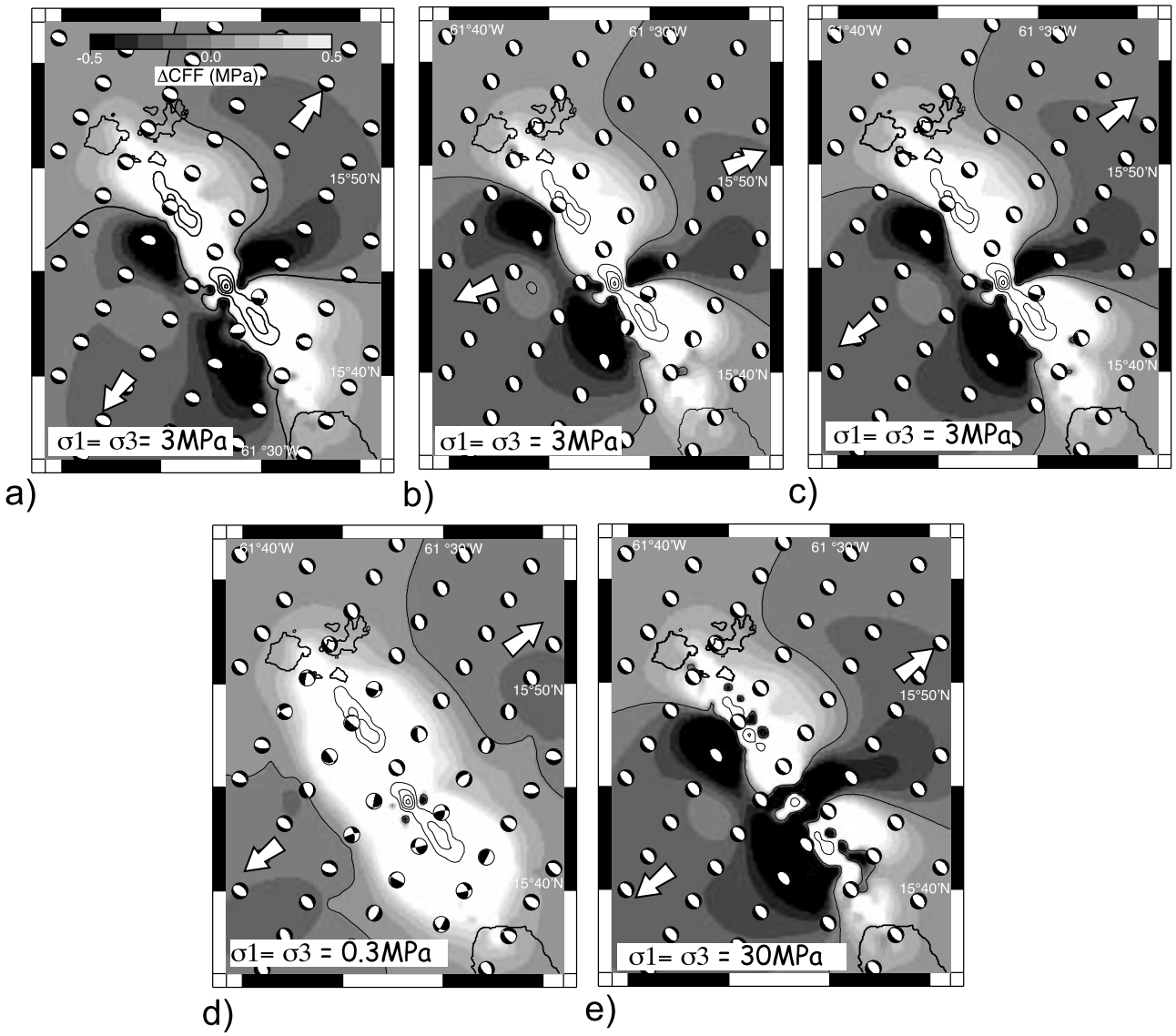

Figure B1. Coulomb stress changes induced by November 21 shock on optimally oriented planes (OOP) by using constant apparent friction model with μ' equal to 0.4 and considering (a) deviatoric regional stress with σ_3 horizontal, N35°E striking and with an amplitude of 3 MPa. σ_1 vertical. (b) As in Figure B1a but with σ_3 striking N65°E. (c) As in Figure B1a but with σ_3 striking N50°E. (d) As in Figure B1c but with amplitude of σ_3 = 0.3 MPa. (e) As in Figure B1c but with amplitude of σ_3 = 30 MPa. Focal mechanisms show motion on SE-dipping OOP. Thin lines: contours with 5 MPa intervals. Dark gray: zones of stress decrease. Light gray: zone of stress increase.

can therefore simulate the expected RSTFs [e.g., *Courboulex et al.*, 1996] corresponding to the source model determined in the previous part. These synthetic RSTFs are shown (red) in Figure A1. The good agreement between observed and synthetic RSTF is a strong indicator of the reality of the source model, and in particular of its main characteristics: the presence of two separated slip zones, activated at the same time after rupture initiation and located on each side of the hypocenter. In fact, as obtained for the observed RSTFs, this source process leads to a clear separation of the pulses related to each ruptured patch for the Northeast stations (PRFA, PIGA). This separation decreases for stations to the North (IPTA, MESA, MOLA), and disappears for the station to the Northwest (GBGA).

Appendix B: Coulomb Stress Modeling

[56] *Cocco and Rice* [2002] showed that the isotropic model yields larger stress changes particularly in off fault lobes for both strike-slip and normal faulting. We calculated the stress changes transferred by the November 21, 2004 earthquake on faults having the same geometry by using the latter model as well as the constant apparent friction model. We used a value of μ' equal to 0.4 which is equivalent to friction values measured in the laboratory and modest fluid

pressure. *King et al.* [1994] and *Cocco et al.* [2000], among others, have shown that the Coulomb stress changes are moderately sensitive to the μ' value. For the isotropic model, μ and B are equal to 0.75 and 0.47, respectively, which corresponds to a μ' value of 0.4. We also test a larger Skempton coefficient of 1. The modeling results show that at the scale of the volume struck by the Les Saintes earthquake, the Coulomb stress changes pattern is not significantly affected by the change of pore pressure model or variation of the Skempton coefficient. Zones of negative or positive coulomb stress changes remain roughly the same. The stress changes are larger when using the isotropic model for μ' and B values corresponding to a μ' value of 0.4. For a higher Skempton coefficient of 1, the stress changes are however slightly smaller.

[57] We calculated the Coulomb stress changes for a deviatoric regional stress tensor assuming that σ_1 is vertical and σ_3 horizontal with orientations ranging between N35°E and N65°E. *King and Cocco* [2001] demonstrated that the stress changes pattern is sensitive to the amplitude of stress only near the master fault for the strike slip case. We calculate the Coulomb stress changes with amplitude of stress ranging between 0.3 and 30 MPa. The results are shown in Figure B1 in map view at mid-depth of the dislocation (5 km). The Coulomb stress changes pattern is almost insensitive to the regional stress orientation at the scale of the aftershock area. It is however very sensitive to the regional stress amplitude. For a weak preexisting stress field (0.3 MPa), the stress change caused by the earthquake rupture is larger than the regional stress close to the fault. In this area, the Coulomb stress changes are positive because the target planes rotate. The focal mechanisms calculated for a weak regional stress near the fault vary between normal strike-slip and reverse faulting. The focal mechanisms calculated for the main aftershocks (Figure 4) are however mostly normal with NNW-SSE striking nodal planes, some showing a slight strike-slip component of motion. This suggests that the regional stress amplitude is likely on the order of few MPa.

Appendix C: Official Letter From City Hall of Terre-de-Haut

[58] We reproduced below the official letter, in French and translation in English, sent on February 2005 by a City Hall employee of Terre-de-Haut in Les Saintes to the Volcanological Observatory of Guadeloupe:

> Un phénomène extraordinaire dans la rade de Terre-De-Haut; une trace blanche de plusieurs centaines de mètres qui ressemble à un bouillonnement de l'eau. Ce phénomène a duré entre 45 min à une heure après le séisme. Il se situe derrière le rocher du Pain de Sucre en direction de l'Îlet Paté. On a l'impression que le phénomène a derivé avec le courant. Certaines personnes parlent d'un bouillonnement plus important juste après le séisme avec de la vapeur d'eau au dessus. (Patrick Bellenus, Mairie de Terre-de-haut).

> An extraordinary phenomenon in the bay of Terre-de-Haut; a several hundred meter long white patch akin to bubbling seawater. This phenomenon lasted 45 min to one hour after the earthquake. It is located behind the Pain-de-Sucre rock in the direction of the Paté islet. The phenomenon seams to have drifted with the current. Some people described more important bubbling just after the earthquake, with vapor above the sea surface. (Patrick Bellenus, City Hall of Terre-de-haut).

[59] **Acknowledgments.** We thank the Institut National des Sciences de l'Univers (France) and Institut de Physique du Globe de Paris for financial support. All actions were coordinated by the seismic emergency cell set up by Vincent Courtillot, director of IPGP, a few hours after the November 2004 earthquake. We are grateful to the Guadeloupe observatory technical staff for their continuous support, especially to Christian Anténor-Habazac, Gilbert Hammouya, Christian Lambert, Bertrand Figaro, and Véronique Daniel-Lurel. We are also grateful to the Guadeloupe authorities and the very hospitable people of Les Saintes for their help. Special thanks go to Jean-Bernard De Chabalier and Alex Nercessian for their prompt scientific and technical interventions during the first weeks of the seismic crisis. We also thank the Dominican Forestry and Wildlife Division, particularly Arlington James who provided crucial information on Boiling Lake water level changes and all the photographs taken between December 2004 and June 2005. We are grateful to Ross S. Stein and three anonymous reviewers for constructive reviews. IPGP contribution 3185.

References

Amelung, F., and G. King (1997), Earthquake scaling laws for creeping and non-creeping faults, *Earth Planet. Sci. Lett.*, *24*(6639), 507–510.

Bazin, S., N. Feuillet, M.-P. Bouin, C. Duclos, M. Bengoubou-Valerius, and J.-B. de Chabalier (2008), The Mw = 7.4 Martinique (Lesser Antilles) intermediate depth earthquake of November 29, 2007: A first analysis, paper presented at the 18th Caribbean Geological Conference, Soc. Dominicana de Geol., Santo Domingo, Dominican Repub., 25–28 March.

Bazin, S., N. Feuillet, C. Duclos, W. Crawford, A. Nercessian, M. Bengoubou-Valerius, F. Beauducel, and S. C. Singh (2010), The 2004–2005 Les Saintes (French West Indies) seismic aftershock sequence observed with ocean bottom seismometers, *Tectonophysics*, *489*(1–4), 91–103.

Beauducel, F., et al. (2005), The Mw 6.3 earthquake of Les Saintes (Guadeloupe) on November 21, 2004, paper presented at European Seismological Commission Annual Workshop, Int. Assoc. of Volcanol. and Chem. of the Earth's Inter., Saint-Claude, Guadeloupe.

Beeler, N. M., R. W. Simpson, S. H. Hickman, and D. A. Lockner (2000), Pore fluid pressure, apparent friction, and Coulomb failure, *J. Geophys. Res.*, *105*, 25533–25542.

Bellon, H. (1988), Reconnaissance chronologique des deux premières phases d'activité volcanique en Dominique, *C. R. Acad. Sci. Ser. II*, *306*, 1487–1492.

Bengoubou-Valerius, M., S. Bazin, D. Bertil, F. Beauducel, and A. Bosson (2008), CDSA: A new seismological data center for the French Lesser Antilles, *Seismol. Res. Lett.*, *79*(1), 90–102.

Bernard, P., and J. Lambert (1988), Subduction and seismic hazard in the northern Lesser Antilles: Revision of the historical seismicity, *Bull. Seismol. Soc. Am.*, *78*, 1965–1983.

Bertil, D., S. Bazin, D. Mallarino, and F. Beauducel (2005), Localisation des principales répliques du séisme des Saintes du 21 Novembre 2004, report, 11 pp., Cent. de Données Sismol. des Antilles, Inst. de Phys. du Globe de Paris, Paris.

Bouchon, M. (1981), A simple method to calculate Green Functions for elastic layered media, *Bull. Seismol. Soc. Am.*, *71*, 959–971.

Bowin, C. (1976), Caribbean Gravity Field and Plate Tectonics, *Spec. Pap. Geol. Soc. Am.*, *169*, 79.

Brodsky, E. E., E. Roeloffs, D. Woodcock, I. Gall, and M. Manga (2003), A mechanism for sustained groundwater pressure changes induced by distant earthquakes, *J. Geophys. Res.*, *108*(B8), 2390, doi:10.1029/2002JB002321.

Cara, M., D. Bertil, N. Feuillet, E. Jacques, P. Tapponnier, P. Guéguen, M. Bengoubou-Valérius, C. Sira, B. Lebrun, and F. Beauducel (2005), Séisme des Saintes (Guadeloupe) du 21 novembre 2004, *Note prélim. BCSF2005-NP3*, 62 pp., Bur.Cent. Sismol. Fr., Strasbourg, France.

Chia, Y., J. Wang, J. Chiu, and L. Chen-Wuing (2001), Changes of groundwater level due to the 1999 Chi-Chi earthquake in the Choshui River alluvial fan in Taiwan, *Bull. Seismol. Soc. Am.*, *91*, 1062–1068.

Cocco, M., and J. R. Rice (2002), Pore pressure and poroelasticity effects in Coulomb stress analysis of earthquake interactions, *J. Geophys. Res.*, *107*(B2), 2030, doi:10.1029/2000JB000138.

Cocco, M., C. Nostro, and G. Ekstrom (2000), Static stress changes and fault interaction during the 1997 Umbria-Marche earthquake sequence, *J. Seismol.*, *4*(4), 501–516.

Courboulex, F., J. Virieux, A. Deschamps, D. Gibert, and A. Zollo (1996), Source investigation of a small event using empirical Green's Functions and simulated annealing, *Geophys. J. Int.*, *125*(3), 768–780.

Delouis, B., D. Giardini, P. Lundgren, and J. Salichon (2002), Joint inversion of InSAR, GPS, teleseismic, and strong-motion data for the spatial and temporal distribution of earthquake slip: Application to the 1999 Izmit mainshock, *Bull. Seismol. Soc. Am.*, *92*, 278–299.

Deplus, C., A. Le Friant, G. Boudon, J. C. Komorowski, B. Villemant, C. Harford, J. Segoufin, and J. L. Cheminee (2001), Submarine evidence for large-scale debris avalanches in the Lesser Antilles Arc, *Earth Planet. Sci. Lett.*, *192*(2), 145–157.

Dorel, J. (1978), Sismicité et structure de l'arc des Petites Antilles et du Bassin Atlantique, Ph.D. thesis, Univ. Paris VI, Paris.

Duclos, C., S. Bazin, W. Crawford, N. Feuillet, A. Nercessian, and S. Singh (2007), Analysis of Les Saintes (Guadeloupe) seismic sequence using ocean bottom seismometers (OBS), paper presented at Genreal Assembly 2007, Eur. Geosci. Union, Vienna.

Dziewonski, A. M., G. G. Ekstrom, and N. N. Maternovskaya (2000), Centroid-moment tensor solutions for October–December, 1999, *Phys. Earth Planet. Inter.*, *121*, 205–221.

Feuillard, M. (1985), Macrosismicité de la Guadeloupe et de la Martinique, report, 348 pp., Inst. de Phys. du Globe de Paris, Paris.

Feuillet, N. (2000), Sismotectonique des Petites Antilles: Liaison entre activité sismique et volcanique, Ph.D. thesis, 283 pp., Univ. Paris VII, Paris.

Feuillet, N., I. Manighetti, and P. Tapponnier (2001), Active arc-transverse normal faulting in Guadeloupe (French Lesser Antilles), *C. R. Acad. Sci. Ser. IIa*, *333*, 583–590.

Feuillet, N., I. Manighetti, P. Tapponnier, and E. Jacques (2002), Arc parallel extension and localization of volcanic complexes in Guadeloupe, Lesser Antilles, *J. Geophys. Res.*, *107*(B12), 2331, doi:10.1029/2001JB000308.

Feuillet, N., P. Tapponnier, I. Manighetti, B. Villemant, and G. C. P. King (2004), Differential uplift and tilt of Pleistocene reef platforms and Quaternary slip rate on the Morne-Piton normal fault (Guadeloupe, French West Indies), *J. Geophys. Res.*, *109*, B02404, doi:10.1029/2003JB002496.

Feuillet, N., et al. (2010), Active faulting induced by slip partitioning in Montserrat and link with volcanic activity: New insights from the 2009 GWADASEIS marine cruise data, *Geophys. Res. Lett.*, *37*, L00E15, doi:10.1029/2010GL042556.

Feuillet, N., F. Beauducel, and P. Tapponnier (2011), Tectonic context of moderate to large historical earthquakes in the Lesser Antilles and mechanical coupling with volcanoes, *J. Geophys. Res.*, doi:10.1029/2011JB008443, in press.

Fournier, N., F. Witham, M. Moreau-Fournier, and L. Bardou (2009), The Boiling Lake of Dominica, West Indies: High temperature volcanic crater lake dynamics, *J. Geophys. Res.*, *114*, B02203, doi:10.1029/2008JB005773.

Girardin, N., M. Feuillard, and J. P. Viode (1991), Regional seismic network in the Lesser Antilles Arc: Shallow seismicity (1981–1988), *Bull. Soc. Geol. Fr.*, *162*(6), 1003–1015.

Harris, R. A. (1998), Introduction to special section: Stress triggers, stress shadows, and implications for seismic hazard, *J. Geophys. Res.*, *103*, 24347–24358.

Hartzell, S. H. (1978), Earthquake aftershocks as Greens Functions, *Geophys. Res. Lett.*, *5*(1), 1–4.

Hill, D. P., F. Pollitz, and C. Newhall (2002), Earthquake-volcano interactions, *Phys. Today*, *55*(11), 41–47.

Institut de Physique du Globe de Paris (IPGP) (2008), Bilan mensuel de l'activité volcanique de la Soufrière de Guadeloupe et de la sismicité régionale, report, Gourbeyre, France.

Jacques, D., and R. C. Maury (1988), Carte géologique du département de la Guadeloupe: Les Saintes, 1/20000, Bur. de Rech. Géol. et Min., Orléans, France.

Jacques, E., J. C. Ruegg, J. C. Lepine, P. Tapponnier, G. C. P. King, and A. Omar (1999), Relocation of M≥2 events of the 1989 Dôbi seismic sequence in Afar: Evidence for earthquake migration, *Geophys. J. Int.*, *138*(2), 447–469.

Jacques, E., T. Kidane, P. Tapponnier, I. Manighetti, Y. Gaudemer, B. Meyer, J. C. Ruegg, L. Audin, and R. Armijo (2011), Normal faulting during the August 1989 earthquakes in central Afar: Sequential triggering and propagation of rupture along the Dôbi Graben, *Bull. Seismol. Soc. Am.*, *101*, 994–1023, doi:10.1785/0120080317.

King, G. C. P. (2007), Fault interaction, earthquake stress changes and the evolution of seismicity, in *Treatise on Geophysics*, vol. 4, edited by G. Schubert, pp. 225–256, Elsevier, Oxford, U. K.

King, G. C. P., and M. Cocco (2001), Fault interaction by elastic stress changes: New clues from earthquake sequences, *Adv. Geophys.*, *44*, 1–38.

King, G. C. P., R. S. Stein, and J. Lin (1994), Static stress changes and the triggering of earthquakes, *Bull. Seismol. Soc. Am.*, *84*, 935–953.

Lee, W. H., and J. H. Lahr (1975), HYPO71 (revisited): A computer program for determining hypocenter, magnitude and first motion pattern of local earthquakes, report, U.S. Geol. Surv., Menlo Park, Calif.

Le Friant, A., P. Heinrich, and G. Boudon (2008), Field survey and numerical simulation of the 21 November 2004 tsunami at Les Saintes (Lesser Antilles), *Geophys. Res. Lett.*, *35*, L12308, doi:10.1029/2008GL034051.

Lindsay, M. J., A. L. Smith, M. J. Roobolt, and M. V. Stasiuk (2005), Dominica, in *Volcanic Hazard Atlas of the Lesser Antilles*, edited by M. Lindsay et al., pp. 1–48, Univ. of the West Indies, St. Augustine, Trinidad and Tobago.

Lopez, A. M., S. Stein, T. Dixon, G. Sella, E. Calais, P. Jansma, J. Weber, and P. LaFemina (2006), Is there a northern Lesser Antilles forearc block?, *Geophys. Res. Lett.*, *33*, L07313, doi:10.1029/2005GL025293.

McCann, W. R. (1985), On the earthquake hazards of Puerto Rico and the Virgin Islands, *Bull. Seismol. Soc. Am.*, *75*, 251–262.

McCann, W. R., J. W. Dewey, A. J. Murphy, and S. T. Harding (1982), A large normal-fault earthquake in the overriding wedge of the Lesser Antilles subduction zone: The earthquake of 8 October 1974, *Bull. Seismol. Soc. Am.*, *72*, 251–262.

Miller, S. A., C. Collettini, L. Chiaraluce, M. Cocco, M. Barchi, and B. J. P. Kaus (2004), Aftershocks driven by a high-pressure CO_2 source at depth, *Nature*, *427*(6976), 724–727.

Muir-Wood, R., and G. C. P. King (1993), Hydrothermal signatures of earthquake strain, *J. Geophys. Res.*, *98*, 22035–22068.

Nabelek, J. (1984), Determination of earthquake fault parameters from inversion of body waves, Ph.D. thesis, Mass. Inst. of Technol., Cambridge.

Noir, J., E. Jacques, S. Bekri, P. M. Adler, P. Tapponnier, and G. C. P. King (1997), Fluid flow triggered migration of events in the 1989 Dôbi earthquake sequence of central Afar, *Geophys. Res. Lett.*, *24*(18), 2335–2338.

Nostro, C., M. Cocco, and M. E. Belardinelli (1997), Static stress changes in extensional regimes: An application to southern Apennines (Italy), *Bull. Seismol. Soc. Am.*, *87*, 234–248.

Nostro, C., R. S. Stein, M. Cocco, M. E. Belardinelli, and W. Marzocchi (1998), Two-way coupling between Vesuvius eruptions and southern Apennine earthquakes, Italy, by elastic stress transfer, *J. Geophys. Res.*, *103*, 24487–24504.

Okada, Y. (1992), Internal deformation due to shear and tensile faults in a half-space, *Bull. Seismol. Soc. Am.*, *82*, 1018–1040.

Quilty, E. G., and E. A. Roeloffs (1997), Water-level changes in response to the 20 December 1994 earthquake near Parkfield, California, *Bull. Seismol. Soc. Am.*, *87*, 310–317.

Reid, H. F., and S. Taber (1920), The Virgin Islands earthquakes of 1867–1868, *Bull. Seismol. Soc. Am.*, *10*, 9–30.

Robson, G. R. (1964), An earthquake catalogue for the eastern Caribbean, *Bull. Seismol. Soc. Am.*, *54*, 785–832.

Roeloffs, E., M. Sneed, D. L. Galloway, M. L. Sorey, C. D. Farrar, J. F. Howle, and J. Hugues (2003), Water-level changes induced by local and distant earthquakes at Long Valley Caldera, California, *J. Volcanol. Geotherm. Res.*, *127*, 269–303.

Salichon, J., A. Lemoine, and H. Aochi (2009), Validation of teleseismic inversion of the 2004 M-w 6.3 Les Saintes, Lesser Antilles, earthquake by 3D finite-difference forward modeling, *Bull. Seismol. Soc. Am.*, *99*, 3390–3401.

Sieh, K. (1996), The repetition of large-earthquake ruptures, *Proc. Natl. Acad. Sci. U. S. A.*, *93*(9), 3764–3771.

Steacy, S., J. Gomberg, and M. Cocco (2005), Introduction to special section: Stress transfer, earthquake triggering, and time-dependent seismic hazard, *J. Geophys. Res.*, *110*, B05S01, doi:10.1029/2005JB003692.

Stein, R. S. (1999), The role of stress transfer in earthquake occurrence, *Nature*, *402*(6762), 605–609.

Stein, S., J. F. Engeln, and D. A. Wiens (1982), Subduction seismicity and tectonics in the Lesser Antilles Arc, *J. Geophys. Res.*, *87*, 8642–8664.

Vallée, M. (2004), Stabilizing the empirical Green Function analysis: Development of the projected Landweber method, *Bull. Seismol. Soc. Am.*, *94*, 394–409.

Villemant, B., and N. Feuillet (2003), Dating open systems by the U-238-U-234-Th-230 method: Application to Quaternary reef terraces, *Earth Planet. Sci. Lett.*, *210*(1–2), 105–118.

Wells, D. L., and K. J. Coppersmith (1994), New empirical relationships among magnitude, rupture length, rupture width, rupture area, and surface displacement, *Bull. Seismol. Soc. Am.*, *84*, 974–1002.

S. Bazin, Norwegian Geotechnical Institute, PO Box 3930 Ulleval Stadion, N-0806 Oslo, Norway.

F. Beauducel, N. Feuillet, E. Jacques, and G. C. P. King, Institut de Physique du Globe de Paris, Sorbonne Paris Cité, UMR 7154 CNRS, Université Paris Diderot, 1 rue Jussieu, F-75238 Paris, CEDEX 05, France. (feuillet@ipgp.fr)

B. Delouis and M. Vallée, GéoAzur, Université de Nice Sophia-Antipolis, IRD, CNRS, OCA, F-06560 Valbonne, France.

P. Tapponnier, Earth Observatory of Singapore, Nanyang Technological University, 50 Nanyang Ave., Block N2-01a-09, 639798, Singapore.